Article

Cell Reports

Targeting Vascular Pericytes in Hypoxic Tumors Increases Lung Metastasis via Angiopoietin-2

Graphical Abstract

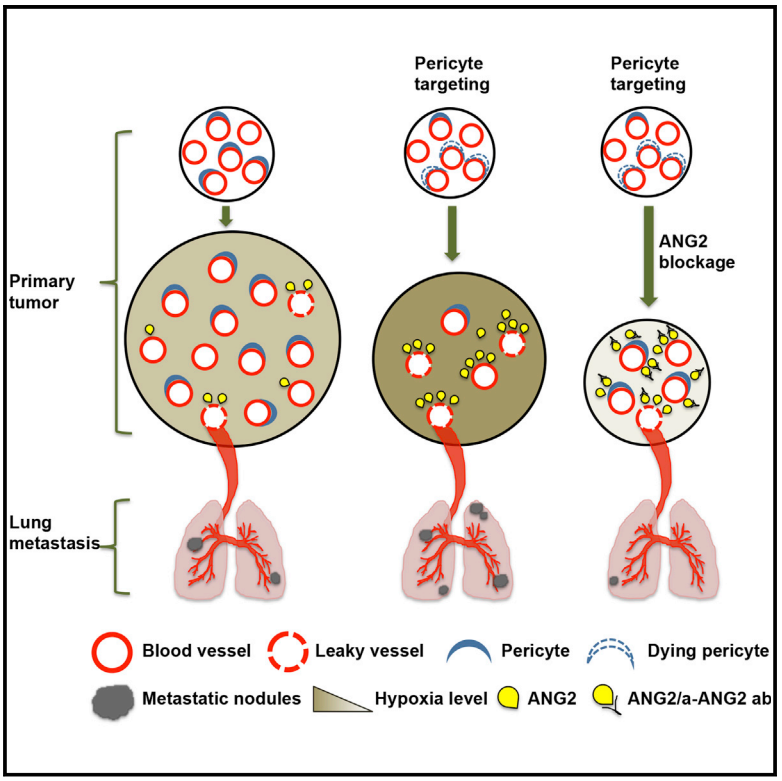

Authors

Doruk Keskin, Jiha Kim, ..., Raghu Kalluri, Valerie S. LeBleu

Correspondence

rkalluri@mdanderson.org (R.K.), vlebleu@mdanderson.org (V.S.L.)

In Brief

Keskin et al. report a tumor-progression-specific role of vascular pericytes in promoting or restricting metastatic disease. Enhanced ANG2 signaling in pericyte-depleted hypoxic tumors promotes vascular defects and metastasis. Using murine models, they show the benefit of ANG2 blockade with vascular targeting therapies in suppressing metastasis.

Highlights

- Pericyte coverage dynamically changes during tumor progression
- Pericyte targeting increases intratumoral hypoxia and lung metastasis
- Vascular defects in pericyte-depleted vessels are mediated by ANG2 upregulation
- ANG2 blockade stabilizes retina and tumor vessels and reduces metastasis

Accession Numbers

GSE55785

Keskin et al., 2015, Cell Reports *10*, 1–16
February 24, 2015 ©2015 The Authors
http://dx.doi.org/10.1016/j.celrep.2015.01.035

CellPress

Please cite this article in press as: Keskin et al., Targeting Vascular Pericytes in Hypoxic Tumors Increases Lung Metastasis via Angiopoietin-2, Cell Reports (2015), http://dx.doi.org/10.1016/j.celrep.2015.01.035

Cell Reports
Article

Targeting Vascular Pericytes in Hypoxic Tumors Increases Lung Metastasis via Angiopoietin-2

Doruk Keskin,[1,2,6] Jiha Kim,[1,4,6] Vesselina G. Cooke,[2] Chia-Chin Wu,[3] Hikaru Sugimoto,[1,2] Chenghua Gu,[4] Michele De Palma,[5] Raghu Kalluri,[1,2,7,*] and Valerie S. LeBleu[1,2,7,*]

[1]Department of Cancer Biology, Metastasis Research Center, University of Texas MD Anderson Cancer Center, Houston, TX 77054, USA
[2]Division of Matrix Biology, Beth Israel Deaconess Medical Center and Harvard Medical School, Boston, MA 02115, USA
[3]Department of Genomic Medicine, University of Texas MD Anderson Cancer Center, Houston, TX 77054, USA
[4]Department of Neurobiology, Harvard Medical School, Boston, MA 02115, USA
[5]The Swiss Institute for Experimental Cancer Research (ISREC), School of Life Sciences, École Polytechnique Fédérale de Lausanne (EPFL), 1015 Lausanne, Switzerland
[6]Co-first author
[7]Co-senior author
*Correspondence: rkalluri@mdanderson.org (R.K.), vlebleu@mdanderson.org (V.S.L.)
http://dx.doi.org/10.1016/j.celrep.2015.01.035

SUMMARY

Strategies to target angiogenesis include inhibition of the vessel-stabilizing properties of vascular pericytes. Pericyte depletion in early-stage non-hypoxic tumors suppressed nascent angiogenesis, tumor growth, and lung metastasis. In contrast, pericyte depletion in advanced-stage hypoxic tumors with pre-established vasculature resulted in enhanced intra-tumoral hypoxia, decreased tumor growth, and increased lung metastasis. Furthermore, depletion of pericytes in post-natal retinal blood vessels resulted in abnormal and leaky vasculature. Tumor transcriptome profiling and biological validation revealed that angiopoietin signaling is a key regulatory pathway associated with pericyte targeting. Indeed, pericyte targeting in established mouse tumors increased angiopoietin-2 (ANG2/*Angpt2*) expression. Depletion of pericytes, coupled with targeting of ANG2 signaling, restored vascular stability in multiple model systems and decreased tumor growth and metastasis. Importantly, *ANGPT2* expression correlated with poor outcome in patients with breast cancer. These results emphasize the potential utility of therapeutic regimens that target pericytes and ANG2 signaling in metastatic breast cancer.

INTRODUCTION

Angiogenesis that accompanies tumor progression provides cancer cells with a means to meet their increased demand for oxygen and nutrients and may also provide a route for cancer cell spread to distal tissues (Folkman, 2002; Zetter, 1998). The complexity of blood vessel growth regulation in tumors may partake in offering adaptive mechanisms to promote rapid emergence of resistance mechanisms in response to anti-angiogenic therapies, thereby limiting their efficacy (Vasudev and Reynolds, 2014). Inhibition of angiogenesis has been shown to suppress metastasis in some experimental tumors (Folkman, 2002; Kirsch et al., 2000; Mazzieri et al., 2011; O'Reilly et al., 1994, 1997; Weidner et al., 1991), whereas in other studies it has been associated with enhanced intratumoral hypoxia and increased local tumor invasion and frequency of metastasis (Cooke et al., 2012; Ebos et al., 2009; Pàez-Ribes et al., 2009). Previously, we reported that the depletion of pericytes in established tumors impaired the neovascularization response and suppressed tumor growth, but enhanced tumor hypoxia and cancer cell spread to target organs of metastasis (Cooke et al., 2012). While pericyte coverage in established tumor blood vessels may function as a gatekeeper of metastasis, the molecular mechanisms mediating the increased frequency of metastasis after pericyte targeting remain poorly characterized.

Pericytes are important regulators of angiogenesis and vascular stability in both developmental and pathological contexts (Armulik et al., 2005, 2011; Bergers and Song, 2005; Hirschi and D'Amore, 1996). These specialized perivascular mesenchymal cells are embedded in the basement membrane of blood vessels (Armulik et al., 2011; Strasser et al., 2010) and secrete pro-angiogenic factors at the onset of angiogenesis (Bergers and Song, 2005; Bergers et al., 2003; Lu et al., 2007; Sennino et al., 2007; Song et al., 2005), while also establishing quiescence of endothelial cells and stabilizing mature blood vessels (Benjamin et al., 1998; Greenberg et al., 2008; Hammes et al., 2002; Nasarre et al., 2009; Orlidge and D'Amore, 1987). Such apparently opposed functions of pericytes are controlled by the evolving pericyte-endothelial cell crosstalk that occurs during tumor angiogenesis. Pericyte-endothelial cell signaling involves multiple pathways, including angiopoietin signaling (Armulik et al., 2005; Armulik et al., 2011). At its core, Angiopoietin-1 (ANG1/*Angpt1*) and angiopoietin-2 (ANG2/*Angpt2*) are ligands for the endothelial receptor TIE2. ANG1 is mainly secreted by pericytes, fibroblasts, and cancer cells (Buchanan et al., 2012) and plays a key role in regulating blood vessel

Please cite this article in press as: Keskin et al., Targeting Vascular Pericytes in Hypoxic Tumors Increases Lung Metastasis via Angiopoietin-2, Cell Reports (2015), http://dx.doi.org/10.1016/j.celrep.2015.01.035

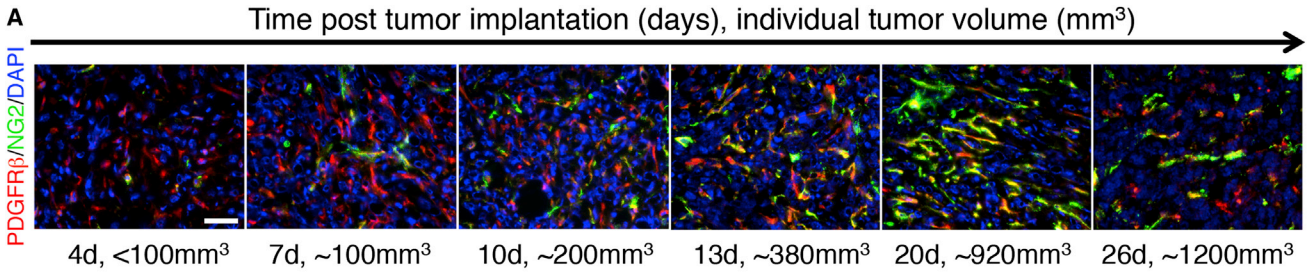

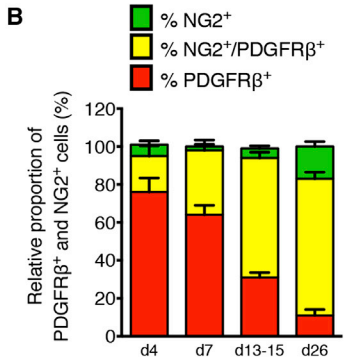

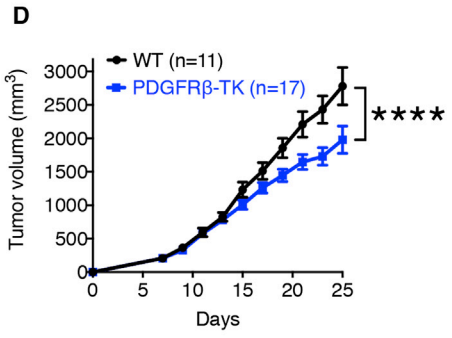

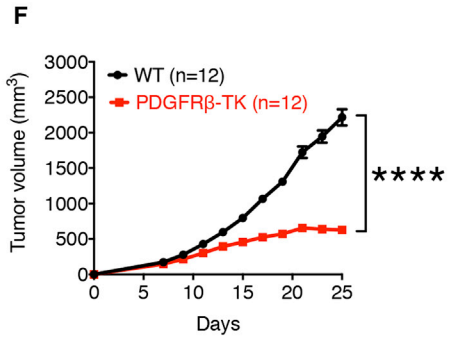

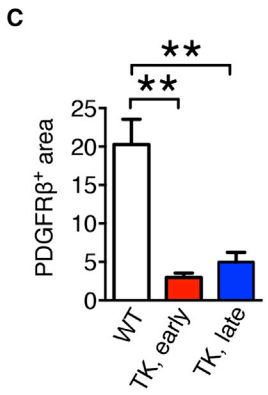

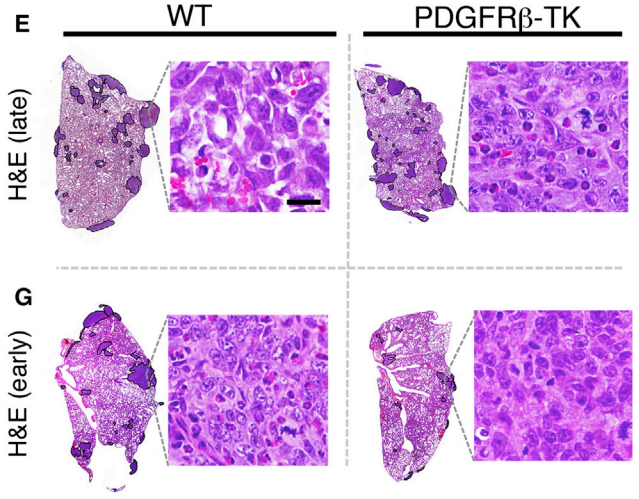

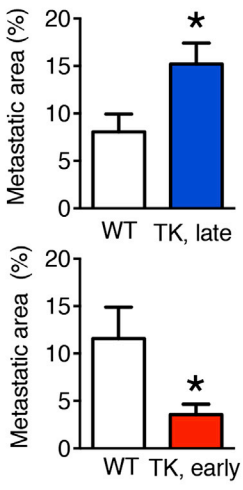

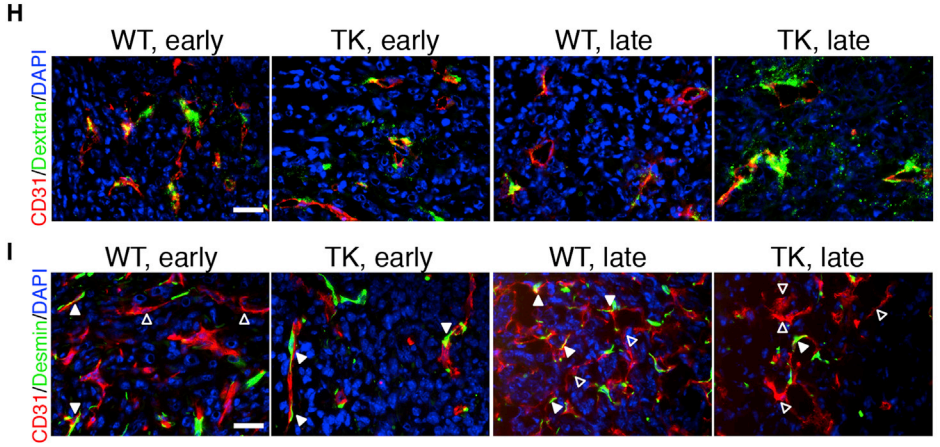

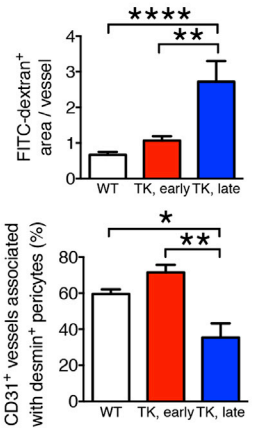

(legend on next page)

permeability. ANG1 also signals to enhance blood vessel stability by increasing the number of vessel-associated pericytes, i.e., pericyte coverage (Augustin et al., 2009; Fuxe et al., 2011; Gaengel et al., 2009; Thurston et al., 1999, 2000). ANG2, which is largely produced by activated endothelial cells, antagonizes ANG1 and destabilizes blood vessels by promoting pericyte detachment and initiating endothelial cell sprouting (Augustin et al., 2009; Scharpfenecker et al., 2005; Thomas and Augustin, 2009). Hypoxia increases ANG2 expression (Kelly et al., 2003; Oh et al., 1999; Rigamonti et al., 2014; Skuli et al., 2012) and ANG2 induces abnormal angiogenesis in the presence of VEGF-A (Augustin et al., 2009; Lobov et al., 2002; Thomas and Augustin, 2009). ANG2 blockade was reported recently to limit the onset of tumor resistance to VEGF-A signaling inhibition in RIP1-Tag2 pancreatic neuroendocrine tumors (Rigamonti et al., 2014).

To gain a better understanding of pericytes and pericyte-endothelial cell interactions and signaling in blood vessel formation, we performed experiments using genetic and pharmacologic targeting of pericytes at various stages of tumor and developmental (retinal) angiogenesis. In an effort to unravel the mechanisms of resistance to anti-vascular therapies, we focused on elucidating the regulatory cellular signaling pathways and functional contribution of pericytes to blood vessel formation during tumor progression.

RESULTS

Coverage and Functional Role of Pericytes Evolve during Tumor Progression

Anti-PDGFRβ and NG2 antibodies have been used to label pericytes (Song et al., 2005). Time-course analysis of pericyte labeling in orthotopically implanted 4T1 mouse mammary tumors showed PDGFRβ$^+$ pericytes starting 4 days after injection of cancer cells (d4). PDGFRβ$^+$ pericyte numbers increased as the tumor grew (d7, d13–15, d26), and their proportion relative to NG2$^+$ pericytes was higher in early-stage non-hypoxic (smaller) tumors when compared to late-stage hypoxic tumors (Figures 1A, 1B, and S1A). Here, we refer to non-hypoxic tumors as early-stage and hypoxic tumors as late stage. Fewer NG2$^+$ pericytes, compared to PDGFRβ$^+$ pericytes, were observed in the early-stage tumors, and the overlap of NG2 and PDGFRβ expression increased as tumors grew, resulting in a gradual increase in the PDGFRβ$^+$/NG2$^+$ double-positive cells with tumor progression (Figures 1A, 1B, and S1A). Thus, growing tumors present with dynamic pericyte coverage defined by sequential and partly overlapping PDGFRβ and NG2 expression.

To functionally address the role of pericytes at different stages of tumor progression, 4T1 breast cancer cells were injected orthotopically into mammary fat pads of NG2-tymidine kinase (TK), PDGFRβ-TK, or wild-type (WT) control mice. We previously showed that daily ganciclovir (GCV) administration specifically depletes proliferating NG2$^+$ and PDGFRβ$^+$ pericytes in NG2-TK and PDGFRβ-TK mice, respectively (Cooke et al., 2012). Depletion of 75.4% of PDGFRβ$^+$ pericytes (Figures 1C and S1B) in advanced-stage tumors (initiated when the average tumor burden was greater than 500 mm^3 and intratumoral hypoxia clearly detected (Figure S1C)) significantly slowed tumor growth (Figure 1D). We previously reported that depletion of NG2$^+$ pericytes in advanced-stage tumors also decreased tumor growth (Cooke et al., 2012).

Depleting pericytes at an advanced tumor stage in NG2-TK and PDGFRβ-TK mice decreased the tumor volume by 60% (Cooke et al., 2012) and 25% (Figure 1D), respectively, and significantly increased the lung metastatic burden (Figure 1E; Cooke et al., 2012). In contrast, pericyte depletion early during tumor growth (Figures 1F and S1B) and prior to the onset of intratumoral hypoxia (Figure S1C) reduced the tumor mass by 36% and 72% in NG2-TK and PDGFRβ-TK mice, respectively (Figures 1F and S1D), but significantly decreased the incidence of lung metastasis only in PDGFRβ-TK mice (Figures 1G and S1E). The difference in the lung metastatic burden noted in the early pericyte depletion setting between NG2-TK and PDGFRβ-TK mice may be due to the important contribution of PDGFRβ$^+$ pericytes to tumor angiogenesis at early stages of tumor growth, when NG2$^+$ pericytes are still scarce (Figures 1A

Figure 1. Pericyte Depletion at Early and Late Stages of Tumor Progression Differentially Impacts Tumor Growth and Metastasis

(A) Double immunolabeling for PDGFRβ and NG2 (pericytes markers) in 4T1 tumors from wild-type (WT) mice at 4, 7, 10, 13, 20, and 26 days after cancer cell orthotopic injection. Scale bar represents 25 μm.

(B) Quantification of NG2$^+$ and PDGFRβ$^+$ cells in individual 4T1 orthotopic tumors over the course of cancer progression. The relative proportion of single- and double-positive cells are reported with 100% reflecting all of the NG2$^+$ and PDGFRβ$^+$ cells per field of view. d4, n = 3; d7, n = 3; d13–15, n = 3; d26, n = 5.

(C) Quantification of the relative PDGFRβ$^+$ area in tumors with early and late PDGFRβ$^+$ pericyte depletion. WT, n = 8; PDGFRβ-TK early (TK, early), n = 5; PDGFRβ-TK late (TK, late), n = 4.

(D) Tumor volume measurements over time, late PDGFRβ$^+$ pericyte depletion. GCV treatment started when total tumor burden reached 500 mm^3.

(E) H&E staining of lungs from WT and PDGFRβ-TK mice with late PDGFRβ$^+$ cell depletion and respective quantification of the percentage lung metastatic area. WT, n = 11; PDGFRβ-TK, n = 17. The metastatic nodules are encircled. High-magnification images of metastatic nodules are shown. Scale bar represents 20 μm.

(F) Tumor volume measurements over time, early PDGFRβ$^+$ pericyte depletion. GCV treatment started before total tumor burden reached 100 mm^3.

(G) H&E staining of lungs from WT and PDGFRβ-TK mice with early PDGFRβ$^+$ cell depletion and respective quantification of the percentage lung metastatic area. WT, n = 12; PDGFRβ-TK, n = 12. High-magnification images of metastatic nodules are shown. Scale bar represents 20 μm.

(H) Representative images of tumors immunolabeled for CD31 and visualization of perfused 2,000 kDa FITC-dextran in the indicated experimental groups and quantitation of FITC-dextran$^+$ area per vessel. WT early, n = 12; PDGFRβ-TK early, n = 7; PDGFRβ-TK late, n = 6. Scale bar represents 25 μm.

(I) Representative images of tumors immunolabeled for CD31 and desmin in the indicated experimental groups and quantification of the percentage of CD31$^+$ vessels associated with desmin-labeling-positive pericytes.

Solid arrowheads, vessels with desmin$^+$ pericyte coverage; empty arrowheads, vessels without desmin$^+$ pericyte coverage. WT n = 6; PDGFRβ-TK early, n = 5; PDGFRβ-TK late, n = 6. Scale bar represents 25 μm. Data are represented as the mean ± SEM. In (D) and (F), two-way ANOVA with Bonferroni's multiple comparison test was used. For (C), (H), and (I), one-way ANOVA with Tukey post hoc analysis was used. Unless otherwise noted, unpaired two-tailed t test was used to determine statistical significance. *p < 0.05, **p < 0.01, ****p < 0.0001. ns, not significant. See also Figure S1.

Please cite this article in press as: Keskin et al., Targeting Vascular Pericytes in Hypoxic Tumors Increases Lung Metastasis via Angiopoietin-2, Cell Reports (2015), http://dx.doi.org/10.1016/j.celrep.2015.01.035

and 1B). PDGFRβ$^+$ pericyte depletion did not affect metastasis in an experimental model of metastatic lung colonization after intravenous injection of 4T1 cancer cells (Figure S1F).

Together, the aforementioned data indicate that PDGFRβ$^+$ pericytes broadly control metastasis of cancer cells at both early and late stages of tumor progression. We therefore focused subsequent studies on PDGFRβ-TK mice and pharmacological targeting of PDGFRβ signaling.

Pericyte Depletion in Advanced-Stage Tumors Is Associated with Compromised Blood Vessel Stability and Enhanced Intratumoral Hypoxia

CD31 labeling of tumor blood vessels was significantly reduced in 4T1 tumors in both early and late pericyte depletion settings (Figure S1G). Intratumoral hypoxia, assayed by immunolabeling for pimonidazole adduct formation following injection of hypoxyprobe, was significantly reduced upon early depletion of pericytes (Figure S1H). In contrast, the smaller tumors in PDGFRβ-TK mice in the late pericyte depletion setting displayed significantly enhanced intratumoral hypoxia compared to WT control tumors (Figure S1H). The increased intratumoral hypoxia noted in the late pericyte depletion setting was associated with an increase in vascular leakage as determined by systemic fluorescein isothiocyanate (FITC)-dextran permeability studies (Figure 1H). A similar degree of permeability was noted in the tumor-associated blood vessels of mice subjected to early pericyte depletion (Figure 1H). The blood vessels in the late depletion setting were deficient in desmin$^+$ cells, representing mature pericytes in structurally stable vessels (Chan-Ling et al., 2004; Kurz et al., 2008; Song et al., 2005; von Tell et al., 2006), suggesting that these vessels were less stable (Figure 1I). The increased intratumoral hypoxia in these tumors was accompanied by enhanced epithelial-to-mesenchymal transition (EMT) in cancer cells, as determined by increased numbers of CK8$^+$ cancer cells acquiring mesenchymal gene expression (αSMA-positive), indicative of enhanced cancer cell invasiveness (Figure S1I).

Differential Effects of Pericyte Depletion on Early and Late Retinal Development

We utilized the retinal vasculature as a model system to further characterize the dynamic functional contributions of PDGFRβ$^+$ pericytes to developmental angiogenesis (Figure 2A). In mouse neonatal pups, retinal blood vessels start forming after birth (P0) and extend from the center to the periphery in an organized network of branches and sprouts, providing an excellent model system to study developmental angiogenesis spatiotemporally (Stahl et al., 2010). To determine the effect of pericyte depletion at early stages of retinal angiogenesis, GCV treatment of PDGFRβ-TK or WT littermate pups was started on the day of birth (P0). Treatment was continued until P5, when the pups were euthanized and the retinas harvested. To assess the effect of pericyte depletion at a later stage of development, when the retina vasculature was partially established, GCV treatment of PDGFRβ-TK or WT littermate pups was initiated at P4 and continued until P9. We noted that very few blood vessels developed in retinas when pericytes were depleted early in PDGFRβ-TK pups compared to WT littermates (Figures 2B and S2A). The lack of type IV collagen immunolabeling, which identifies the vascular basement membrane in the retinas, indicated that the lack of blood vessels after early PDGFRβ$^+$ pericyte depletion was not due to vessel regression but rather impaired angiogenesis (Figure S2B).

When pericyte depletion was delayed, we noted unperturbed blood vessel formation and sprouting angiogenesis, with blood vessels reaching the periphery of the retina (Figures 2C and 2D). In this setting, isolectin B4 staining showed that, although the microvascular area was not detectably affected (Figure 2E), blood vessel branching was significantly reduced (Figure 2F). Severe vascular leakage in both the central remodeling zone and peripheral front of the expanding inner vascular plexus (shown by 70 kDa FITC-dextran perfusion) was apparent after late pericyte depletion (Figures 2G and S2C). The pericyte-depleted blood vessels also appeared dilated, with an enlarged vessel diameter allowing increased perfusion of 2,000 kDa FITC-dextran (Figure S2D). Together, these findings indicate differential effects of depleting pericytes during the early and late stages of retinal development.

Angiopoietin Signaling Is Differentially Modulated by Temporal Pericyte Depletion during Tumor Progression and Retinal Angiogenesis

To identify the potential molecular effectors that may be responsible for enhanced metastasis following the late PDGFRβ$^+$ cell depletion (in contrast to early PDGFRβ$^+$ cell depletion), we compared the gene expression profiles of tumors subjected to either early or late PDGFRβ$^+$ cell depletion. Growth factor signaling pathway analyses coupled to quantitative transcript level measurements revealed that the angiopoietin signaling pathway was deregulated both in the early and late pericyte depletion setting, along with the VEGF, PDGF, and HGF signaling pathways (Figure S3A). While all growth factors and signaling targets evaluated by qRT-PCR showed a similar up- or downregulation in both the early and late pericyte-depleted experimental groups compared to their WT controls (Figures S3B and S3C), *Anpgt1* and *Anpgt2* were uniquely deregulated in the early versus late experimental groups (Figures 3A and 3B). Specifically, in tumors with early pericyte depletion, *Angpt1* transcript levels were elevated by 5-fold while *Angpt2* transcript levels were unchanged (Figure 3A). In contrast, in tumors with late pericyte depletion, *Angpt1* transcript levels were unchanged but *Angpt2* transcript levels were elevated by 3-fold (Figure 3B) and ANG2 protein levels by 3-fold (Figure 3C). This significant deregulation in transcript and protein levels in early versus late pericyte depletion was restricted to ANG1 and ANG2 (Figures 3A and 3B). These results indicate a switch in ANG1/ANG2 expression along with temporal targeting of PDGFRβ$^+$ pericytes in tumors. In situ hybridization (ISH) supported the transcript data; indeed, we found no difference in *Angpt2* signal in the early pericyte depletion setting (versus controls), whereas there was a marked *Angpt2* signal in the late pericyte depletion setting (Figure 3D). *Angpt2* transcripts were detected primarily in foci co-localizing with collagen IV and CD31 immunolabeling, supporting a focal upregulation of *Angpt2* in endothelial cells (Figures 3E and 3F). While most blood vessels displayed high levels of *Angpt2* (Figure 3E, red

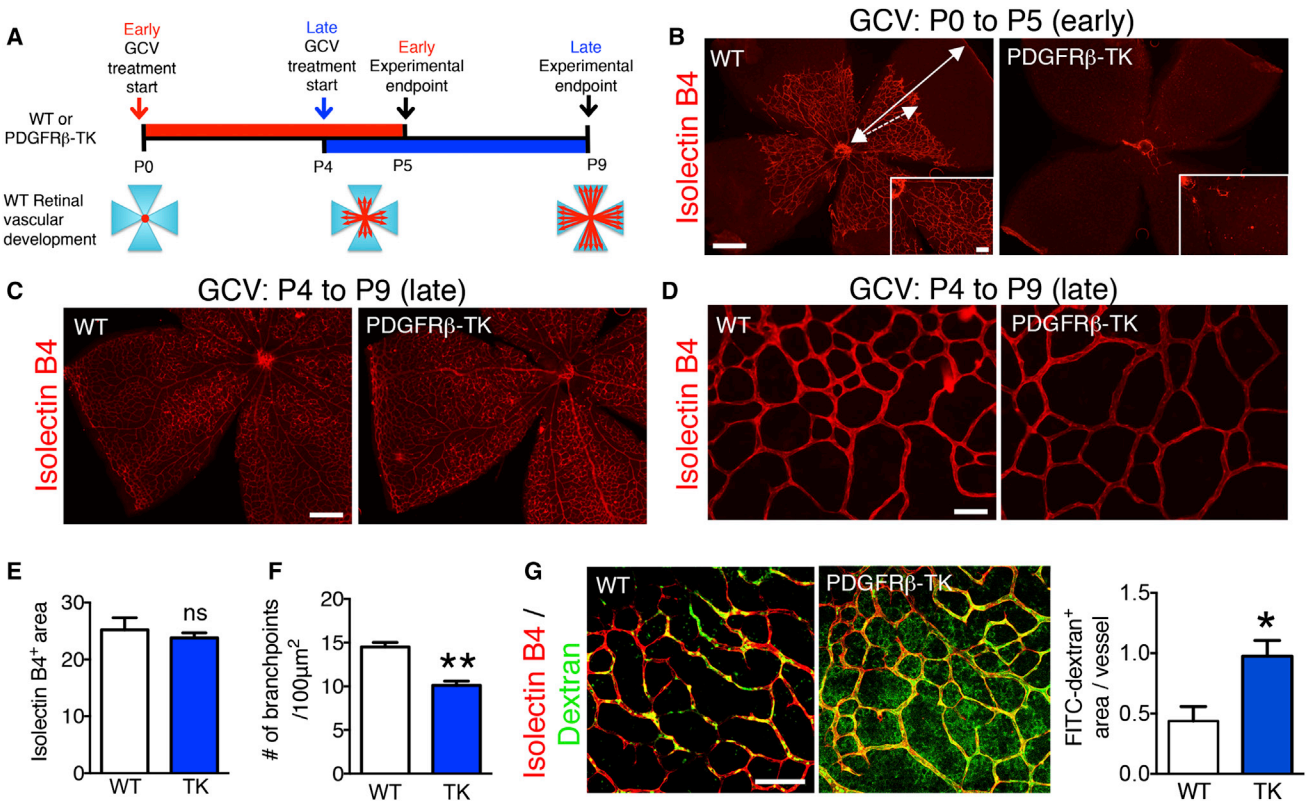

Figure 2. Early, P0–P5, and Late, P4–P9, Pericyte Depletion Differentially Alter Developmental Angiogenesis in the Mouse Retina

(A) Schematic representation of stage-specific pericyte depletion in the development of the retina vasculature.

(B) Isolectin B4 staining of retinas from P5 WT and PDGFRβ-TK pups treated with GCV from P0 to P5 (early depletion). Scale bar represents 500 μm; inset scale bar represents 100 μm. Dashed arrow shows the extent of vessel coverage in WT retina at P5 with respect to the edge of the retina (solid arrow).

(C and D) Isolectin B4 staining of retinas from WT and PDGFRβ-TK mice treated with GCV from P4 to P9 (late depletion). Scale bars represent 500 μm (C) and 100 μm (D).

(E) Quantitation of the isolectin $B4^+$ area/field (vessel area). WT, n = 4; PDGFRβ-TK, n = 3.

(F) Quantitation of the number of branch points/100 μm^2. WT, n = 4; PDGFRβ-TK, n = 3.

(G) Isolectin B4 staining and visualization of 70 kDa FITC-dextran in WT and PDGFRβ-TK mice treated with GCV from P4 to P9 and quantitation of FITC-$dextran^+$ area per vessel. WT, n = 3; PDGFRβ-TK, n = 5. Scale bar represents 100 μm.

Data are represented as the mean ± SEM. Unpaired two-tailed t test was used to determine statistical significance. *$p < 0.05$, **$p < 0.01$. ns, not significant. See also Figure S2.

arrowheads), a few blood vessels lacked *Angpt2* expression (Figure 3E, white arrowheads).

Differential expression of *Angpt1* and *Angpt2* associated with pericyte depletion was also analyzed in the retina angiogenesis model. Late depletion of retinal pericytes (P4–P7) showed unchanged *Angpt1* transcript levels, whereas *Angpt2* expression was increased (Figure 3G). Overall, these results indicate an inversed ANG1/ANG2 expression pattern in association with temporal targeting of $PDGFR\beta^+$ pericytes during both tumor growth and retinal angiogenesis.

Anti-ANG2 Antibody Treatment Restores the Integrity of Pericyte-Depleted Leaky Blood Vessels and Reduces Metastasis

To determine whether the increase in lung metastasis observed in 4T1 mammary tumor-bearing PDGFRβ-TK mice was due to increased ANG2 expression in tumors with late pericyte depletion, we performed rescue experiments using a murinized anti-ANG2 neutralizing antibody (Srivastava et al., 2014). Control mice were treated with an isotype-matched immunoglobulin G (IgG) antibody. In WT mice without pericyte depletion, anti-ANG2 only moderately reduced tumor growth rate (Figure 4A). Pericyte depletion was initiated when tumor burden reached 500 mm^3 of volume, and this produced a significant reduction in tumor growth rate (Figure 4A). Although the anti-ANG2 antibody did not affect the tumor growth rate in pericyte-depleted tumors (Figure 4A), we observed a significant reduction in the frequency of lung metastasis (Figures 4B and 4D). Specifically, lung metastasis trended toward a decrease in WT mice treated with anti-ANG2, and the increased lung metastasis in PDGFRβ-TK mice was abated to levels observed in WT mice treated with the anti-ANG2 antibody (Figures 4B and 4D).

Next, we assayed the impact of anti-ANG2 treatment on vascular leakage and intratumoral hypoxia. We found that anti-ANG2 treatment in the context of $PDGFR\beta^+$ pericyte depletion restored the structural stability of the blood vessels, as

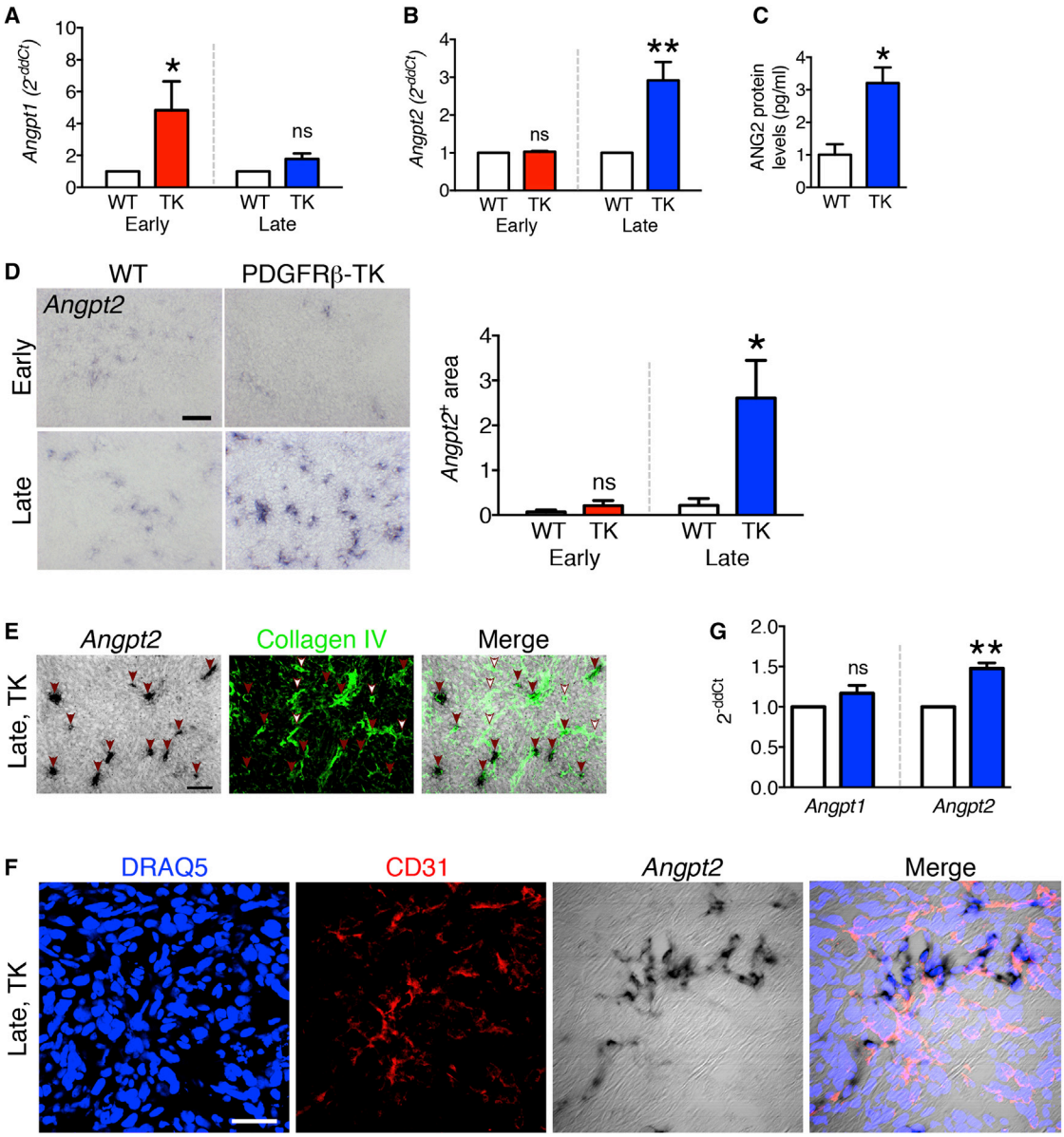

Figure 3. Angiopoietin-1 and Angiopoietin-2 Expression Is Differentially Modulated by Pericyte Depletion in a Tumor-Stage-Dependent Manner

(A and B) Transcript levels of *Angpt1* (A) and *Angpt2* (B) in 4T1 tumors from WT and PDGFRβ-TK mice with early and late pericyte depletion. *Angpt1*: WT early, n = 6; PDGFRβ-TK early, n = 6; WT late, n = 5; PDGFRβ-TK late, n = 7. *Angpt2*: WT early, n = 6; PDGFRβ-TK early, n = 4; WT late, n = 5; PDGFRβ-TK late, n = 7. The control group (WT) was arbitrarily set to 1, unpaired one-tailed t test.

(C) ANG2 protein levels in tumors from WT (n = 4) and PDGFRβ-TK (n = 4) mice with late pericyte depletion.

(D) *Angpt2 in situ* hybridization on the frozen section of 4T1 tumors from WT and PDGFRβ-TK mice with either early or late pericyte depletion and quantification of *Angpt2*$^+$ area/field of view. WT early, n = 6; PDGFRβ-TK early, n = 4; WT late, n = 6; PDGFRβ-TK late, n = 5. Scale bar represents 50 μm. One-way ANOVA was used to determine statistical significance.

(E) *Angpt2 in situ* hybridization followed by collagen IV immunolabeling in tumors from PDGFRβ-TK mice with late pericyte depletion. Red arrowheads, *Angpt2*/collagen IV double-positive vessels. White arrowheads, collagen IV positive vessels that lack *Angpt2* expression. Scale bar represents 50 μm.

(F) *Angpt2 in situ* hybridization followed by CD31 immunolabeling in tumors from PDGFRβ-TK mice (late pericyte depletion). Scale bar represents 20 μm.

(G) Transcript levels of *Angpt1* and *Angpt2* in retinas upon late pericyte depletion (P4-P7). *Angpt1*: WT, n = 4; PDGFRβ-TK, n = 7. *Angpt2*: WT, n = 4; PDGFRβ-TK, n = 7. The control group was arbitrarily set to 1, unpaired one-tailed t test.

Data are represented as the mean ± SEM. Unless otherwise indicated, unpaired two-tailed t test was used to determine statistical significance. *$p < 0.05$, **$p < 0.01$. ns, not significant. See also Figure S3 and Table S1.

determined by reduced vascular leakage (Figures 4E and 4F), restored vessel diameter (Figures S4A and S4B), and diminished EMT program (Figures 4G, 4H, S4D, and S4E) and intratumoral hypoxia (Figures 4I–4J). Tumor lymphangiogenesis (mostly peri-tumoral in this model) assayed by LYVE-1 staining was unchanged in all experimental groups (Figure S4F). Pericyte depletion, with and without anti-ANG2 treatment, did not impact vascular TIE2 expression (Figure S4G), nor tumor infiltration by TIE2-expressing macrophages (Figure S4H), suggesting that ANG2 upregulation in pericyte-depleted tumors acts in an autocrine manner to destabilize endothelial cells, and that the effect of anti-ANG2 treatment is mediated by suppression of the imbalanced ANG2/TIE2 signaling without affecting TIE2 expression in endothelial cells or macrophages. Finally, global gene expression profiling of the WT, PDGFRβ-TK, and PDGFRβ-TK tumors treated with the anti-ANG2 antibody revealed impaired angiopoietin signaling in pericyte-depleted tumors, and a gene expression pattern partially reverted to that of WT control mice after treatment with the anti-ANG2 antibody (Figure 4K).

Then, we analyzed ANG2 signaling induced by late PDGFRβ$^+$ cell depletion during retinal angiogenesis. Similar to the findings in tumors, anti-ANG2 rescued the vascular phenotype observed in the retina of PDGFRβ-TK pups. The enhanced vascular leakage at the central zone of the vascular plexus and at the sprouting edge of the primary plexus was observed specifically in PDGFRβ-TK mice in the late-stage pericyte depletion setting; anti-ANG2 antibody treatment re-established the retinal vessel structural stability in PDGFRβ-TK mice (Figures 5A and 5B). Enhanced vessel diameter in PDGFRβ-TK mice (Figure S3D) was also restored by anti-ANG2 (Figure 5C). Anti-ANG2 treatment did not modify NG2$^+$ pericyte coverage in retinal blood vessels (Figures 5A and 5D). Taken together, these results indicate that PDGFRβ$^+$ pericyte depletion promotes an ANG2-mediated increase in vascular destabilization and permeability, both in tumors and the developing retinal vasculature.

Treatment of Established Breast Tumors with Imatinib and Anti-ANG2 Antibody Restores Blood Vessel Structural Stability and Limits Metastasis

We previously reported that imatinib significantly reduced pericyte coverage in 4T1 tumors (Cooke et al., 2012). In larger tumors (tumor burden ~500 mm^3), imatinib treatment mirrored the phenotype observed in PDGFRβ-TK and NG2-TK mice, which resulted in increased vascular leakage and intratumoral hypoxia associated with lung-enhanced metastasis (Cooke et al., 2012). To determine whether imatinib and ANG2 neutralization may synergistically decrease primary tumor burden and lung metastasis, we treated 4T1 tumor-bearing mice with a single agent (imatinib) or a combination therapy (imatinib and anti-ANG2). Control mice were treated with saline (PBS) and control IgG.

Single therapy with imatinib reduced primary tumor growth compared to control mice (Figure 6A), as previously reported (Cooke et al., 2012). Combination therapy with imatinib and anti-ANG2 antibody further increased inhibition of primary tumor growth when compared to imatinib monotherapy (Figure 6A). Imatinib treatment in established 4T1 tumors resulted in an increase in lung metastasis (Figures 6B and 6C; Cooke et al., 2012); however, the combination therapy resulted in a significant reduction of lung metastasis when compared to imatinib only (Figures 6B and 6C). Tumor necrosis was increased by anti-ANG2 (Figure 6D), as previously reported (Thomas et al., 2013), and may contribute to the stalled tumor growth (Figure 6A).

Histological findings in the heart, bowel, kidney, and pancreas were unremarkable in control, imatinib alone, and imatinib/anti-ANG2 combination therapy (Figure S5A). A liver metastasis was noted in one of the mice treated with imatinib (in agreement with enhanced metastatic disease after imatinib monotherapy), and enlarged spleen with follicular expansion characteristic of tumor bearing mice was observed in all mice (Figure S5A).

Intratumoral hypoxia and vascular leakage were enhanced in tumors treated with imatinib (Figures 6E and 6F; Cooke et al., 2012). Concomitant anti-ANG2 and imatinib treatment reduced intratumoral hypoxia (Figure 6E), vascular leakage (Figure 6F), and vessel diameter (Figures S4A and S4C). Additional targets of imatinib, such as c-Kit and Abl1, were unchanged in imatinib-treated mice (Figure S5B; Cooke et al., 2012). Collectively, these results indicate that the anti-metastatic effects of ANG2 blockade may be due, at least in part, to improved vascular stabilization and decreased tumor hypoxia.

Normalization of Angiopoietin Signaling in PDGFRβ$^+$ Pericyte-Depleted Tumors Promotes Desmin$^+$ Pericyte Coverage and Increases Endothelial Cell-Cell Tight Junctions

To determine the mechanistic underpinning of ANG2 neutralization in decreasing destabilized blood vessels in the context of genetic (PDGFRβ-TK mice, see Figures 4 and 5) or pharmacologic (imatinib, see Figure 6) targeting of PDGFRβ$^+$ pericytes, we evaluated the differential expression of the mature pericyte marker desmin (*Des*). Gene expression profiling showed a sustained decrease in *Pdgfrb* transcript levels in tumors with PDGFRβ-TK mice despite anti-ANG2 antibody treatment (Figure 7A). ANG2 blockade limited the decrease in *Des* transcript levels observed in tumors of PDGFRβ-TK compared to control mice (Figure 7A). Desmin immunolabeling in proximity to CD31 vascular labeling indicated a significant increase in desmin$^+$ mature pericyte coverage of tumor vessels in PDGFRβ$^+$ pericyte-depleted tumors treated with the anti-ANG2 antibody (Figure 7B). ANG2 blockade also promoted desmin$^+$ pericyte coverage of tumor vessels in WT mice without PDGFRβ$^+$ pericyte depletion (Figure 7B). These results show that anti-ANG2 treatment upregulated the expression of desmin and increased vascular coverage by mature pericytes, in spite of the loss of *Pdgfrb* expression caused by genetic targeting of PDGFRβ$^+$ pericytes.

Global gene expression signaling revealed partially restored VEGF family-ligand-receptor interactions and CXCR4 signaling pathways after anti-ANG2 treatment (Figure 7C). Transcriptome analyses showed that expression of *Cxcr4* was increased in tumors from PDGFRβ-TK compared to WT control mice (both treated with control IgG); these results were validated by qRT-PCR (Figure 7D). *Cxcr4* expression in tumors from PDGFRβ-TK mice treated with anti-ANG2 antibody was restored to levels observed in WT tumors (Figure 7D). These results suggest a rescued vessel permeability defect following anti-ANG2 antibody treatment. *Angpt2* transcript levels were elevated in

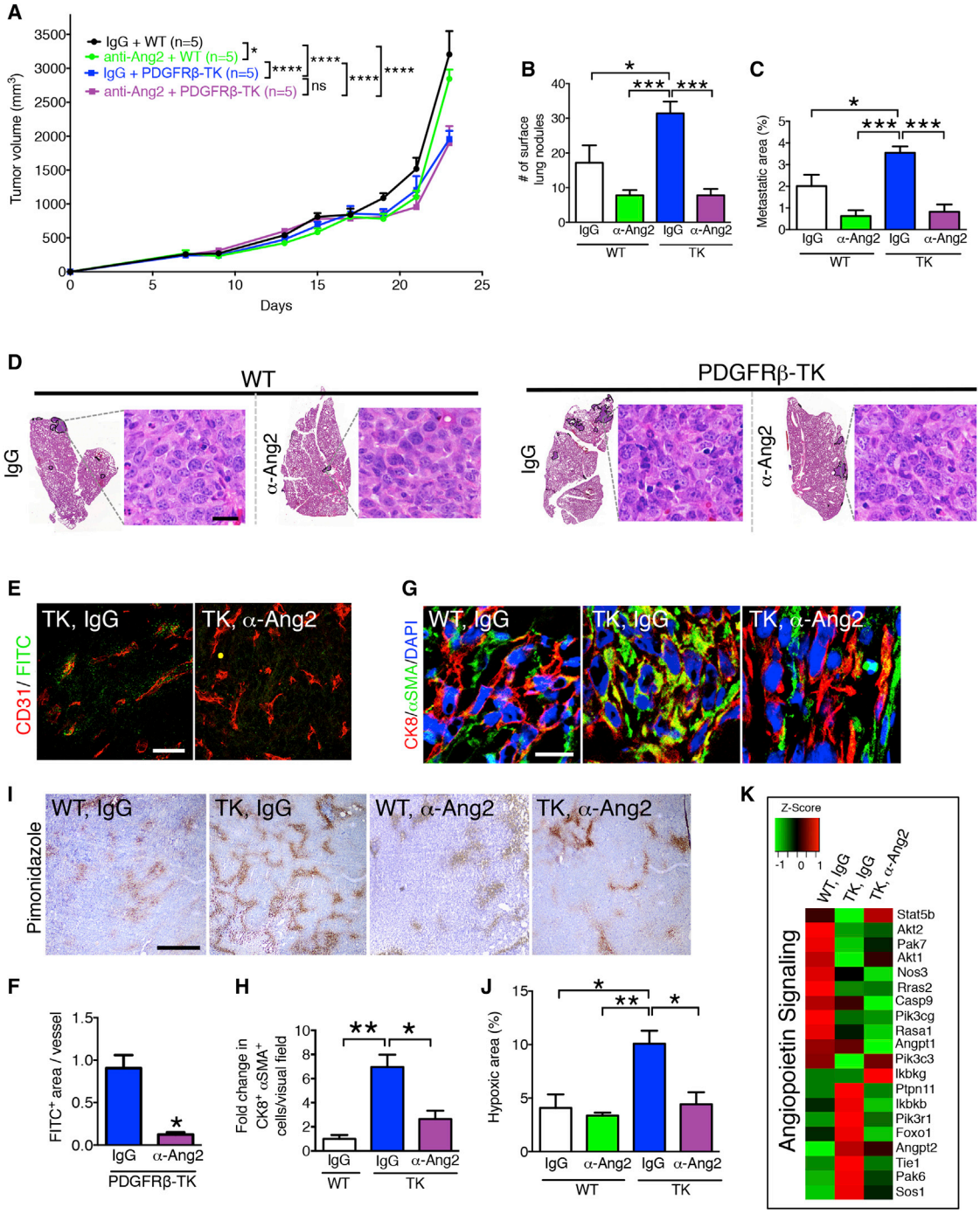

Figure 4. Anti-ANG2 Antibody Treatment In Pericyte-Depleted Tumors Restores Vascular Integrity and Reduces Lung Metastasis

(A) Tumor volume measurements over time in indicated experimental groups (IgG: control for anti-ANG2 antibody treatment). All mice were treated with ganciclovir (GCV) concurrently with the indicated treatment and treatment started when total tumor burden reached 500 mm^3. Two-way ANOVA with Tukey's multiple comparison test was used.

(B) Quantification of the number of surface lung nodules. IgG + WT, n = 5; anti-ANG2 + WT, n = 5; IgG + PDGFRβ-TK, n = 5; anti-ANG2 + PDGFRβ-TK, n = 5.

(C) Quantification of the percentage lung metastatic area based on H&E staining of lung sections. IgG + WT, n = 5; anti-ANG2 + WT, n = 5; IgG + PDGFRβ-TK, n = 5; anti-ANG2 + PDGFRβ-TK, n = 5.

(D) H&E staining of lungs from the indicated experimental groups. The metastatic nodules are encircled. High-magnification images of metastatic nodules are shown. Scale bar represents 20 μm.

(legend continued on next page)

PDGFRβ-TK tumors, corroborating our earlier observation (Figures 3A–3C). Anti-ANG2 treatment did not suppress the transcription of *Angpt2*, consistent with previous findings (Mazzieri et al., 2011; Rigamonti et al., 2014), indicating that the therapeutic effect of antibody-mediated ANG2 blockade is mediated through downstream signaling rather than via transcriptional feedback downregulation of *Angpt2* (Figure 7D). These transcriptomic analyses support the notion that increased *Angpt2* expression in tumors with late pericyte depletion may compromise vessel integrity via deregulation of CXCR4/CXCL12 signaling. Several studies have shown that CXCR4/CXCL12 plays a role in vascular permeability (Suri et al., 1998), endothelial cell patterning and morphology (Strasser et al., 2010), and transendothelial migration and metastasis of breast cancer cells (Lee et al., 2004; Mukherjee and Zhao, 2013; Müller et al., 2001). We also observed restored ZO-1 expression (a marker for endothelial tight junction) in endothelial cells of tumors from PDGFRβ-TK mice treated with the anti-ANG2 antibody, similar to levels of control tumors (WT mice treated with IgG control) (Figure 7E).

ANGPT2 and PDGFRB Expression Correlate with Poor Outcome in Patients with Breast Cancer

We queried the Kaplan-Meier plotter data set (Gyorffy et al., 2012) and evaluated the survival probability of patients with breast cancer based on their tumor transcriptomes (Figures 7F–7H). The median transcript level of *ANGPT1*, *ANGPT2*, and *PDGFRB* was used to stratify 3,455 patient tumor transcriptomes into high and low expression for each gene. High *ANGPT1* expression was associated with improved outcome (Figure 7F). In contrast, a significant association of high *ANGPT2* expression and poor recurrence free survival was found (Figure 7G). In addition, low *PDGFRB* expression was associated with poor recurrence free survival (Figure 7H). These analyses are in agreement with results obtained in our mouse studies: whereas high *ANGPT1* was associated with suppressed metastasis, high *ANGPT2* was associated with enhanced metastasis in mice (Figures 1E and 3B–3D). These results are also consistent with the higher metastatic tumor burden noted in PDGFRβ-TK mice (low *PDGFRB*), in which high *ANGPT2* expression was noted (Figures 3B–3D).

DISCUSSION

Anti-angiogenic cancer therapies show efficacy but did not realize the full potential that preclinical studies had suggested, highlighting an unforeseen complexity of tumor neo-angiogenesis (Bisacchi et al., 2003; Folkman, 1972). Newly formed blood vessels, or lack thereof, affect the metabolic status of the primary tumor and may influence cancer cells' metastatic potential in addition to providing routes to metastasis (Cooke et al., 2012; Folkman, 2002; Zetter, 1998). To shed light on the complex and dynamic nature of pericyte-endothelial cell interactions in various phases of tumor angiogenesis, we employed genetic targeting of pericytes in non-hypoxic (early stage) or hypoxic (advanced stage) tumors.

Our data indicated that anti-vascular therapy via depletion of PDGFRβ$^+$ pericytes at early stages of tumor progression reduced metastasis, whereas targeting these cells at later stages enhanced metastasis. The stage-specific effects are a result of differential, dynamic PDGFRβ$^+$ pericyte interactions with endothelial cells during the evolving angiogenic process. Early PDGFRβ$^+$ pericyte depletion severely suppressed tumor angiogenesis, blunted primary tumor growth, and reduced intratumoral hypoxia. The desmin$^+$ pericyte coverage in the small, PDGFRβ$^+$ pericyte-depleted tumors suggests that impeded tumor angiogenesis at this early stage of tumor growth was associated with the development of a vascular network that adequately matched the tumor's energetic needs with its growth rate.

In contrast with the early pericyte depletion experiments, the late depletion of pericytes in established primary tumors resulted in a moderate decrease of tumor growth but was associated with a significant increase of lung metastasis. The late pericyte-depleted tumors displayed an overall reduction of tumor blood vessels, with the remaining blood vessels characterized by hyperpermeability and poor desmin$^+$ pericyte coverage, both likely contributing to the increased intratumoral hypoxia and metastatic dissemination. The stage-specific metastasis phenotypes may also underscore the relative contribution of specific pericyte subtypes to tumor angiogenesis. Our studies on early tumor development indeed showed a differential timing for PDGFRβ$^+$ and NG2$^+$ pericytes accumulation, with increasing overlap of expression, suggesting that PDGFRβ$^+$ cells acquire NG2 expression. These findings may explain, at least in part, the differences observed in early ablation of PDGFRβ$^+$ versus NG2$^+$ cells in 4T1 tumors, whereby early ablation of NG2$^+$ cells has minimal effects on tumor growth and metastasis.

Our transcriptomic studies identified angiopoietin signaling as uniquely deregulated with respect to early versus late pericyte targeting, and we further implicated ANG2 expression and signaling as a key mediator of the metastatic phenotype associated with tumor-stage-specific PDGFRβ$^+$ pericyte depletion. Using genetic depletion of PDGFRβ$^+$ pericytes or

(E and F) Immunolabeling for CD31 and FITC for visualization of 2,000 kDa FITC-dextran in the indicated experimental groups and quantification of the FITC$^+$ area per field of view. IgG + PDGFRβ-TK, n = 3; anti-ANG2 + PDGFRβ-TK, n = 3. Scale bar represents 50 μm. Unpaired two-tailed t test was used.
(G and H) Representative images of tumors immunolabeled for CK8 and αSMA in the indicated experimental groups and quantification of the relative CK8$^+$ αSMA$^+$ cells per visual field. WT, n = 3; PDGFRβ-TK, n = 3; anti-ANG2+PDGFRβ-TK, n = 3. Scale bar represents 10 μm.
(I and J) Immunolabeling of hypoxyprobe (pimonidazole adduct formation) in the indicated experimental groups and quantitation of relative percentage hypoxic area. IgG + WT, n = 3; anti-ANG2 + WT, n = 3; IgG + PDGFRβ-TK, n = 4; anti-ANG2 + PDGFRβ-TK, n = 3. Scale bar represents 500 μm.
(K) Heatmap of the differentially regulated genes in the angiopoietin signaling pathways in the tumors of indicated experimental groups. Data are represented as the mean ± SEM.
Unless otherwise noted, one-way ANOVA with Tukey post hoc analysis was used to determine statistical significance. *$p < 0.05$, **$p < 0.01$, ***$p < 0.001$, ****$p < 0.0001$. See also Figure S4.

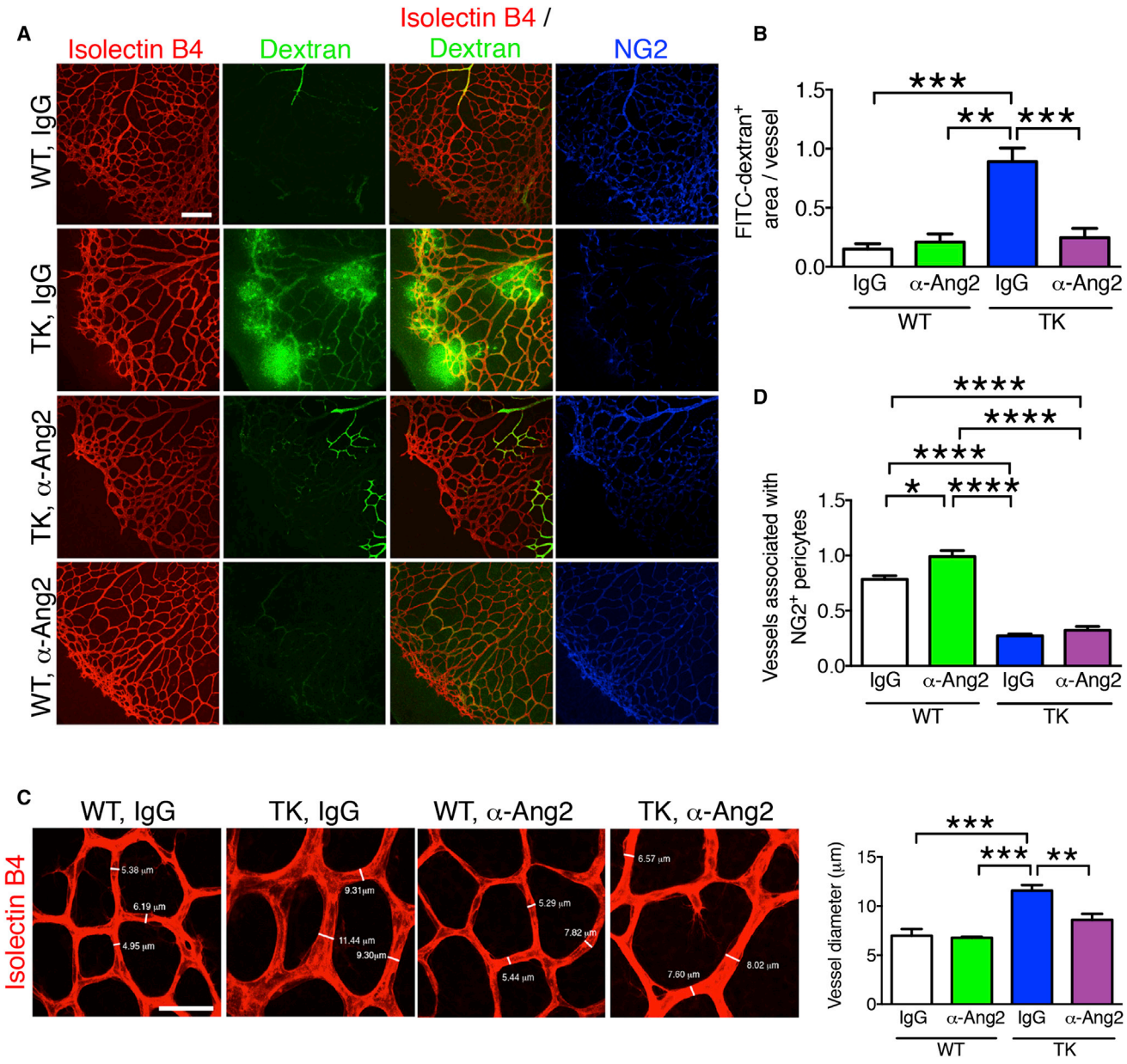

Figure 5. Anti-ANG2 Antibody Treatment Reduces Vascular Leakage of Retinas with Late Pericyte Depletion

(A) Immunolabeling for NG2, isolectin B4 staining, and visualization of 2,000 kDa FITC-dextran of retinas from WT and PDGFRβ-TK pups treated with either control IgG or anti-ANG2 antibody from P4 to P9 (late pericyte depletion). All mice were treated with GCV. Scale bar represents 200 μm.

(B) Quantification of FITC-dextran$^+$ area per vessel. IgG + WT, n = 3; anti-ANG2 + WT, n = 3; IgG + PDGFRβ-TK, n = 3; anti-ANG2 + PDGFRβ-TK, n = 5.

(C) Isolectin B4 staining of the retina in the indicated experimental groups and quantification of the mean vessel diameter. IgG + WT, n = 3; anti-ANG2 + WT, n = 4; IgG + PDGFRβ-TK, n = 5; anti-ANG2 + PDGFRβ-TK, n = 5. Representative vessel diameters are listed. Scale bar represents 40 μm.

(D) Quantification of Isolectin B4$^+$ vessels associated with NG2$^+$ pericytes coverage. IgG + WT, n = 3; anti-ANG2 + WT, n = 4; IgG + PDGFRβ-TK, n = 3; anti-ANG2 + PDGFRβ-TK, n = 5.

Data are represented as the mean ± SEM. One-way ANOVA with Tukey post hoc analysis was used to determine statistical significance. *$p < 0.05$, **$p < 0.01$, ***$p < 0.001$, ****$p < 0.0001$.

pharmacological targeting of PDGFRβ signaling by imatinib, we showed that the leaky vascular phenotype in these tumors was associated with elevated ANG2 expression. Vessels with increased ANG2 stimulation in the Rip1Tag2 transgenic mouse model were previously characterized by reduced pericyte coverage and were found dilated, destabilized, and highly permeable (Fagiani et al., 2011), all of which are consistent with our observations. Furthermore, our analyses also highlighted a deregulation of CXCR4/CXCL12 signaling in association with late PDGFRβ$^+$ pericytes depletion, also in concordance

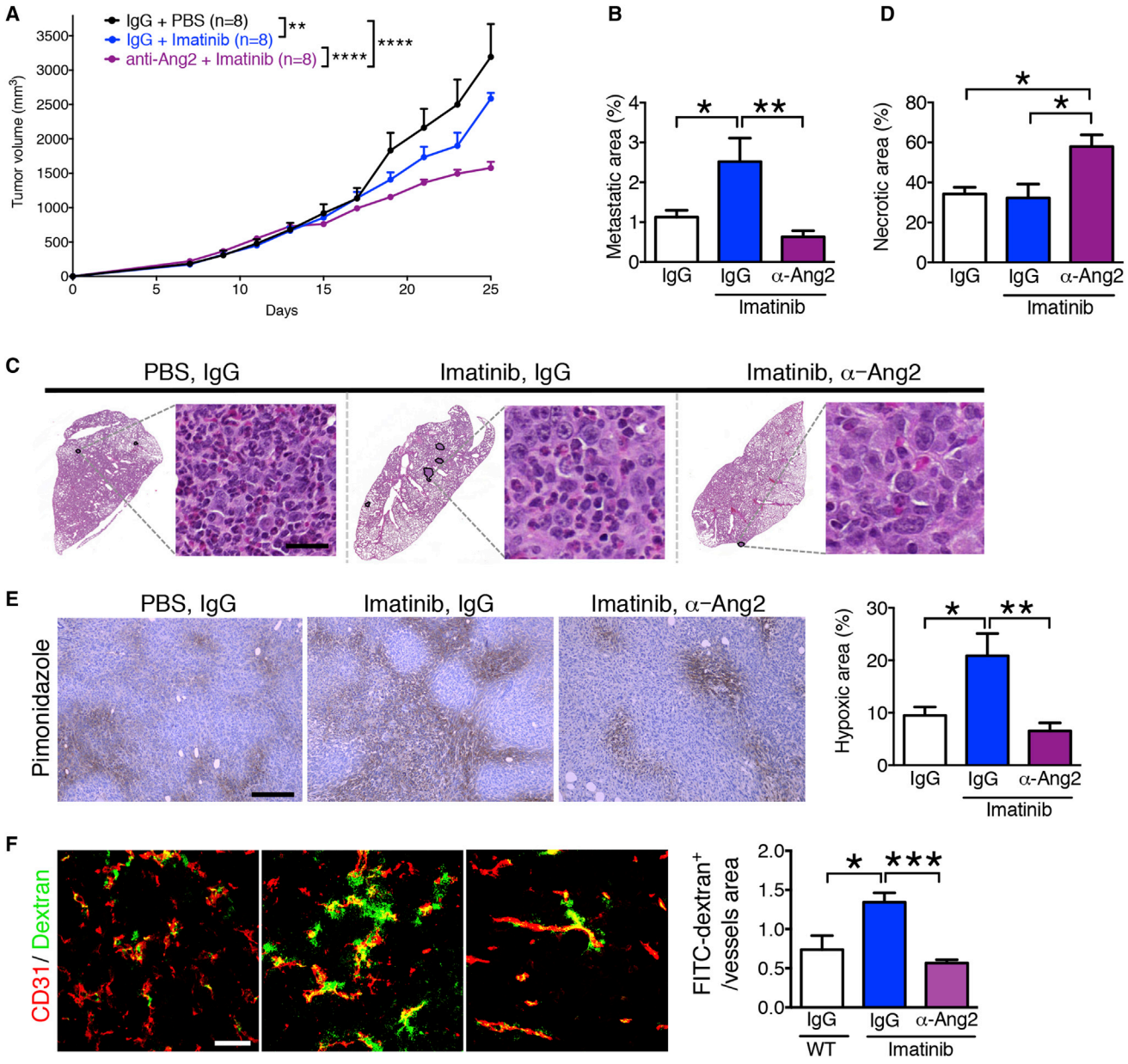

Figure 6. Imatinib and Anti-ANG2 Antibody Treatments Synergistically Control Tumor Growth and Metastasis

(A) Tumor volume measurements over time in indicated experimental groups (IgG: control for anti-ANG2 treatment, PBS: control for imatinib). Treatment started when total tumor burden reached 500 mm^3. Two-way ANOVA with Bonferroni's multiple comparison test was used.

(B) Quantification of the percentage lung metastatic area. IgG + PBS, n = 8; IgG + imatinib, n = 8; anti-ANG2 + imatinib, n = 8.

(C) H&E staining of lungs from the indicated experimental groups. The metastatic nodules are encircled. High-magnification images of metastatic nodules are shown; scale bar represents 20 μm.

(D) Quantification of the percentage tumor necrotic area. IgG + PBS, n = 5; IgG + imatinib, n = 5; anti-ANG2 + imatinib, n = 5.

(E) Immunolabeling of hypoxyprobe (pimonidazole adduct formation) in the indicated experimental groups and quantitation of percentage hypoxic area. IgG + PBS, n = 5; IgG + imatinib, n = 5; anti-ANG2 + imatinib, n = 5. Scale bar represents 500 μm.

(F) Immunolabeling for CD31 and visualization of 2,000 kDa FITC-dextran in the indicated experimental groups and quantification of the FITC-dextran$^+$ area per vessel. IgG + PBS, n = 3; IgG + imatinib, n = 5; anti-ANG2 + imatinib, n = 5. Scale bar represents 50 μm.

Data are represented as the mean ± SEM. Unless otherwise noted, one-way ANOVA with Tukey post hoc analysis was used to determine statistical significance. *p < 0.05, **p < 0.01, ***p < 0.001. See also Figure S6.

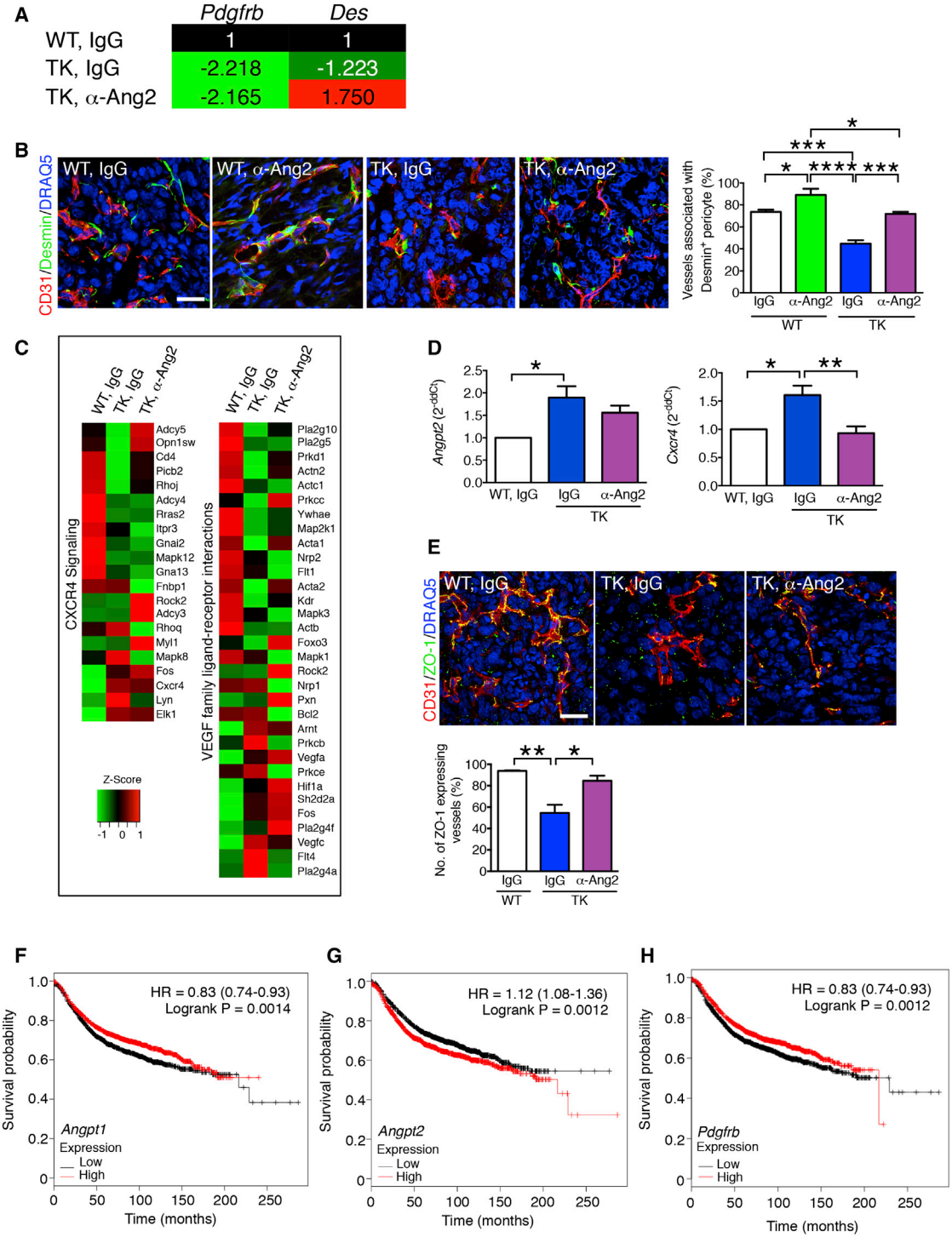

Figure 7. Neutralization of ANG2 in Pericyte-Depleted Tumors Re-establish Mature Pericyte Vessel Coverage and Endothelial Cell-Cell Tight Junction in Association with Restored CXCR4 and VEGF Signaling Pathways

(A) Color-coded table listing the fold change in transcript levels of *Pdgfrb* and *Des* (desmin) based on global gene expression profiling of tumors from mice in the indicated experimental groups.

(B) Representative images of tumors immunolabeled for CD31 and desmin in the indicated experimental groups and quantification of the percentage $CD31^+$ vessels associated with $desmin^+$ pericytes. IgG + WT, n = 3; anti-ANG2 + WT, n = 3; IgG + PDGFRβ-TK, n = 4; anti-ANG2 + PDGFRβ-TK, n = 4. Scale bar represents 25 μm.

(C) Heatmaps reflecting the differentially regulated genes in tumors of indicated experimental groups in each of the indicated pathways.

(legend continued on next page)

with its known implication in vessel permeability (Suri et al., 1998) and breast cancer cell transendothelial migration and metastasis (Lee et al., 2004; Mukherjee and Zhao, 2013; Müller et al., 2001). Our previous studies have shown that pericyte targeting in established tumors leads to increased EMT associated with increased c-MET expression in hypoxic cancer cells (Cooke et al., 2012). The current study suggests that such increase in c-MET expression in cancer cells could be facilitated by enhanced hypoxia resulting from ANG2-mediated vascular defects.

Our results indicate ANG2-mediated destabilization of sprouting blood vessels in the hypoxic environment of the late pericyte depletion setting, and high levels of *Angpt2* in this setting may be restricted to endothelial cells in the more hypoxic regions of the tumor. ANG2 has been associated with metastasis in melanoma patients; indeed, increased circulating ANG2 levels were associated with tumor progression and metastasis (Helfrich et al., 2009). The association of ANG1 with metastasis has been uncertain in clinical contexts (Szarvas et al., 2008). Our results indicate that ANG1 expression is associated with decreased metastasis and increased desmin$^+$ pericyte coverage, and high *ANGPT1* is associated with increased survival probability in surveyed breast cancer transcriptomes.

While overexpression of ANG2 increases metastasis through enhanced vascular permeability (Holopainen et al., 2012), blocking of ANG2 signaling enhances pericyte coverage of blood vessels (Rigamonti et al., 2014) and strongly inhibits metastasis (Mazzieri et al., 2011), possibly by stabilizing the tumor-associated vasculature via enhanced endothelial cell-cell junctions (Holopainen et al., 2012) and by displacing macrophages that assist cancer cell intravasation from the tumor blood vessels (Mazzieri et al., 2011). Of note, anti-ANG2 suppresses both spontaneous metastasis of primary mammary tumors and the metastatic colonization of the lung after cancer cell seeding (Mazzieri et al., 2011). In this regard, anti-ANG2 antibody treatment was recently shown to suppress metastatic growth also in the adjuvant (post-surgical) setting in mice, an effect mediated via suppression of the endothelial cell proinflammatory phenotype at the metastatic site (Srivastava et al., 2014). While such anti-metastatic mechanism could also be at play in our studies, we also show that ANG2 blockade concomitant to PDGFRβ$^+$ pericyte depletion during the late phases of tumor progression provides benefit by reducing both primary tumor growth and metastatic disease. Anti-ANG2 treatment rescued the vascular defects induced by pericyte targeting, and imatinib and anti-ANG2 combination therapy suppressed primary tumor growth and controlled lung metastasis. The vascular defects associated with pericyte targeting in retinal angiogenesis were also restored upon anti-ANG2 therapy. ANG2 signaling inhibition enhanced endothelial cell-cell tight junctions, and these results altogether suggest that ANG2 signaling is central to the loss of vascular stability associated with PDGFRβ$^+$ pericyte targeting in both tumor and developmental angiogenesis. Finally, the analysis of the tumor transcriptomes of patients with breast cancer revealed a robust correlation between recurrence-free survival and expression of *ANGPT2* and *PDGFRB*.

Our results indicate that the enhanced cancer cell dissemination induced by targeting PDGFRβ$^+$ pericytes in advanced stage tumors could be controlled by the administration of an anti-ANG2 antibody. Increased intratumoral hypoxia in late-stage tumors enhances ANG2 production by endothelial cells (Holash et al., 1999; Saharinen et al., 2011), further destabilizing the tumor vasculature and fueling a vicious cycle set forth by PDGFRβ$^+$ pericyte targeting. While the anti-metastatic effects of the anti-ANG2 antibody may also be due to impaired angiogenesis and cancer cell growth at the metastatic site, our results indicate that its effects are also targeted to the primary tumors and their metastatic potential. Our findings further imply that vascular normalization and consequently improved vascular perfusion (Augustin et al., 2009; Carmeliet and Jain, 2011a, 2011b; Jain, 2005; Li et al., 2007; Skuli et al., 2009) may be achieved by PGDFRβ$^+$ pericyte targeting concomitant with anti-ANG2 antibody therapy. This strategy, if combined with chemotherapy, may potently suppress tumor growth by enhancing chemotherapeutic delivery while preserving the structural stability of the tumor blood vessels, thus minimizing hypoxia-induced metastatic dissemination.

EXPERIMENTAL PROCEDURES

Cells and Mice

4T1 Balb/c mammary tumor epithelial cells were obtained from ATCC and grown in DMEM media supplemented with 10% fetal bovine serum (FBS). PDGFRβ-TK and NG2-TK Balb/c mice were previously described (Cooke et al., 2012). Female mice, between the ages of 6 and 12 weeks, were used for orthotopic implantation of 4T1 mammary epithelial cancer cells, as described previously (Cooke et al., 2012). Mice received daily intraperitoneal (i.p.) GCV injections at a 50 mg/kg body weight (BW) dose at the indicated time points and, when indicated, also received i.p. injections of a neutralizing anti-ANG2 antibody (murinized LC06, Roche Diagnostics) (Srivastava et al., 2014) or control isotype-matched IgG antibody once a week (10 mg/kg BW in 0.2 ml PBS), or imatinib or PBS by oral gavage daily (50 mg/kg BW in 0.1 ml). All mouse experiments were reviewed and approved by the Institute of Animal Care and Use Committee at the Beth Israel Deaconess Medical Center (BIDMC) and the MD Anderson Cancer Center (MDACC). Additional experimental details are listed in the Supplemental Experimental Procedures.

Tumor Vessel Leakage and Metastatic Burden

Mice were injected in the retro-orbital venous plexus with 100 μl of 10 mg/ml FITC-dextran (2,000,000 MW, Sigma) 5 min prior euthanasia. Tumor sections from optimum cutting temperature (OCT)-embedded tumors were immunostained for CD31. FITC-dextran was visualized either directly by

(D) qRT-PCR for *Angpt2* and *Cxcr4* in tumors from the indicated experimental groups. *Angpt2*: IgG + WT, n = 4; IgG + PDGFRβ-TK, n = 5; anti-ANG2 + PDGFRβ-TK, n = 5. *Cxcr4*: IgG + WT, n = 4; IgG + PDGFRβ-TK, n = 4; anti-ANG2 + PDGFRβ-TK, n = 4.

(E) Representative images of tumors immunolabeled for CD31 and ZO-1 in the indicated experimental groups and quantification of the percentage of the number of ZO-1$^+$ vessels. IgG + WT, n = 3; IgG + PDGFRβ-TK, n = 3; anti-ANG2 + PDGFRβ-TK, n = 3. Scale bar represents 25 μm.

(F–H) Kaplan-Meier plots depicting the recurrence free survival probability of patients with breast cancer (n = 3,455) based on *Angpt1* (F), *Angpt2* (G), and *Pdgfrb* (H) tumor expression. HR, hazard ratio. Log-rank test was used. Data are represented as the mean ± SEM. Unless otherwise noted, one-way ANOVA with Tukey post hoc analysis was used to determine statistical significance. *p < 0.05, **p < 0.01, ***p < 0.001, ****p < 0.0001.

Please cite this article in press as: Keskin et al., Targeting Vascular Pericytes in Hypoxic Tumors Increases Lung Metastasis via Angiopoietin-2, Cell Reports (2015), http://dx.doi.org/10.1016/j.celrep.2015.01.035

fluorescent microscopy under the green fluorescent filter or by immunostaining with anti-FITC antibody and a FITC-conjugated secondary antibody. FITC-dextran is quantified by ImageJ area fraction analysis. Multiple sections/tumor were analyzed at original magnification ×40 with $n \geq 3$ tumors/group. Histological assessment and quantitation of the metastatic and tumor necrosis areas are described in the Supplemental Experimental Procedures.

Microarray Analysis and qPCR Analyses

Microarray analysis was performed using Mouse Ref8 or Ref6 Gene Expression BeadChip (Illumina). Details for microarray samples, qRT-PCR analyses, and primer sequence information are listed in the Supplemental Experimental Procedures and Table S1.

Statistical Analysis

For comparison between two groups with one grouping variable, the unpaired two-tailed Student's t test was used. For RT-PCR analyses, the unpaired one-tailed Student's t test was used to compare dCt between experimental groups. To compare multiple groups, analysis of variance (ANOVA) was used with Prism software. For multiple groups with one grouping variable, one-way ANOVA with multiple comparisons with Tukey correction was performed, and, for multiple groups with two grouping variables, two-way ANOVA with Bonferroni's multiple comparison test was used. $p < 0.05$ was considered statistically significant. All data are represented as the mean with error bars corresponding to SEM.

ACCESSION NUMBERS

The NCBI GEO accession number for the gene expression data reported in this paper is GSE55785.

SUPPLEMENTAL INFORMATION

Supplemental Information includes Supplemental Experimental Procedures, five figures, and one table and can be found with this article online at http://dx.doi.org/10.1016/j.celrep.2015.01.035.

AUTHOR CONTRIBUTIONS

D.K., J.K., V.G.C., C.-C.W., H.S., and V.S.L. performed experiments and analyzed data. M.D.P. provided reagents and intellectual input and edited the manuscript. C.G. provided reagents and intellectual input. D.K. and J.K. participated in the writing the manuscript and preparation of figures. R.K. and V.S.L. wrote the manuscript, prepared figures, and oversaw the study design and execution and analysis of the experiments.

ACKNOWLEDGMENTS

We wish to thank Markus Thomas and Joachim Muller (Roche, Penzberg, Germany) for providing the anti-ANG2 antibody and Lauren Bizarro, Cristina Espinosa da Silva, and Laura Gibson for genotyping and animal husbandry support. We thank Erica Lawson, Komal Vadnagara, Donna Lundy, Sergio Dias, and Oleg Tsinkalovsky for technical support. We also wish to thank Dr. Balázs Győrffy for his help in mining the KM plotter data sets. This study was primarily supported by the NIH grant CA155370 (R.K.). R.K. is also supported by the Cancer Prevention and Research Institute of Texas and the Metastasis Research Center at MD Anderson Cancer Center, NIH grants CA125550, CA155370, CA151925, and CA163191. V.S.L. is supported by the NIH/NCI CCSG New Faculty Award P30CA016672 and UT MDACC Khalifa Bin Zayed Al Nahya Foundation. C.G. is supported by NIH RO1 NS064583.

Received: September 29, 2014
Revised: December 2, 2014
Accepted: January 13, 2015
Published: February 19, 2015

REFERENCES

Armulik, A., Abramsson, A., and Betsholtz, C. (2005). Endothelial/pericyte interactions. Circ. Res. *97*, 512–523.

Armulik, A., Genové, G., and Betsholtz, C. (2011). Pericytes: developmental, physiological, and pathological perspectives, problems, and promises. Dev. Cell *21*, 193–215.

Augustin, H.G., Koh, G.Y., Thurston, G., and Alitalo, K. (2009). Control of vascular morphogenesis and homeostasis through the angiopoietin-Tie system. Nat. Rev. Mol. Cell Biol. *10*, 165–177.

Benjamin, L.E., Hemo, I., and Keshet, E. (1998). A plasticity window for blood vessel remodelling is defined by pericyte coverage of the preformed endothelial network and is regulated by PDGF-B and VEGF. Development *125*, 1591–1598.

Bergers, G., and Song, S. (2005). The role of pericytes in blood-vessel formation and maintenance. Neuro-oncol. *7*, 452–464.

Bergers, G., Song, S., Meyer-Morse, N., Bergsland, E., and Hanahan, D. (2003). Benefits of targeting both pericytes and endothelial cells in the tumor vasculature with kinase inhibitors. J. Clin. Invest. *111*, 1287–1295.

Bisacchi, D., Benelli, R., Vanzetto, C., Ferrari, N., Tosetti, F., and Albini, A. (2003). Anti-angiogenesis and angioprevention: mechanisms, problems and perspectives. Cancer Detect. Prev. *27*, 229–238.

Buchanan, C.F., Szot, C.S., Wilson, T.D., Akman, S., Metheny-Barlow, L.J., Robertson, J.L., Freeman, J.W., and Rylander, M.N. (2012). Cross-talk between endothelial and breast cancer cells regulates reciprocal expression of angiogenic factors in vitro. J. Cell. Biochem. *113*, 1142–1151.

Carmeliet, P., and Jain, R.K. (2011a). Molecular mechanisms and clinical applications of angiogenesis. Nature *473*, 298–307.

Carmeliet, P., and Jain, R.K. (2011b). Principles and mechanisms of vessel normalization for cancer and other angiogenic diseases. Nat. Rev. Drug Discov. *10*, 417–427.

Chan-Ling, T., Page, M.P., Gardiner, T., Baxter, L., Rosinova, E., and Hughes, S. (2004). Desmin ensheathment ratio as an indicator of vessel stability: evidence in normal development and in retinopathy of prematurity. Am. J. Pathol. *165*, 1301–1313.

Cooke, V.G., LeBleu, V.S., Keskin, D., Khan, Z., O'Connell, J.T., Teng, Y., Duncan, M.B., Xie, L., Maeda, G., Vong, S., et al. (2012). Pericyte depletion results in hypoxia-associated epithelial-to-mesenchymal transition and metastasis mediated by met signaling pathway. Cancer Cell *21*, 66–81.

Ebos, J.M., Lee, C.R., Cruz-Munoz, W., Bjarnason, G.A., Christensen, J.G., and Kerbel, R.S. (2009). Accelerated metastasis after short-term treatment with a potent inhibitor of tumor angiogenesis. Cancer Cell *15*, 232–239.

Fagiani, E., Lorentz, P., Kopfstein, L., and Christofori, G. (2011). Angiopoietin-1 and -2 exert antagonistic functions in tumor angiogenesis, yet both induce lymphangiogenesis. Cancer Res. *71*, 5717–5727.

Folkman, J. (1972). Anti-angiogenesis: new concept for therapy of solid tumors. Ann. Surg. *175*, 409–416.

Folkman, J. (2002). Role of angiogenesis in tumor growth and metastasis. Semin. Oncol. *29* (6, Suppl 16), 15–18.

Fuxe, J., Tabruyn, S., Colton, K., Zaid, H., Adams, A., Baluk, P., Lashnits, E., Morisada, T., Le, T., O'Brien, S., et al. (2011). Pericyte requirement for anti-leak action of angiopoietin-1 and vascular remodeling in sustained inflammation. Am. J. Pathol. *178*, 2897–2909.

Gaengel, K., Genové, G., Armulik, A., and Betsholtz, C. (2009). Endothelial-mural cell signaling in vascular development and angiogenesis. Arterioscler. Thromb. Vasc. Biol. *29*, 630–638.

Greenberg, J.I., Shields, D.J., Barillas, S.G., Acevedo, L.M., Murphy, E., Huang, J., Scheppke, L., Stockmann, C., Johnson, R.S., Angle, N., and Cheresh, D.A. (2008). A role for VEGF as a negative regulator of pericyte function and vessel maturation. Nature *456*, 809–813.

Gyorffy, B., Lánczky, A., and Szállási, Z. (2012). Implementing an online tool for genome-wide validation of survival-associated biomarkers in ovarian-cancer using microarray data from 1287 patients. Endocr. Relat. Cancer *19*, 197–208.

Hammes, H.P., Lin, J., Renner, O., Shani, M., Lundqvist, A., Betsholtz, C., Brownlee, M., and Deutsch, U. (2002). Pericytes and the pathogenesis of diabetic retinopathy. Diabetes *51*, 3107–3112.

Helfrich, I., Edler, L., Sucker, A., Thomas, M., Christian, S., Schadendorf, D., and Augustin, H.G. (2009). Angiopoietin-2 levels are associated with disease progression in metastatic malignant melanoma. Clin. Cancer Res. *15*, 1384–1392.

Hirschi, K.K., and D'Amore, P.A. (1996). Pericytes in the microvasculature. Cardiovasc. Res. *32*, 687–698.

Holash, J., Wiegand, S.J., and Yancopoulos, G.D. (1999). New model of tumor angiogenesis: dynamic balance between vessel regression and growth mediated by angiopoietins and VEGF. Oncogene *18*, 5356–5362.

Holopainen, T., Saharinen, P., D'Amico, G., Lampinen, A., Eklund, L., Sormunen, R., Anisimov, A., Zarkada, G., Lohela, M., Heloterä, H., et al. (2012). Effects of angiopoietin-2-blocking antibody on endothelial cell-cell junctions and lung metastasis. J. Natl. Cancer Inst. *104*, 461–475.

Jain, R.K. (2005). Normalization of tumor vasculature: an emerging concept in antiangiogenic therapy. Science *307*, 58–62.

Kelly, B.D., Hackett, S.F., Hirota, K., Oshima, Y., Cai, Z., Berg-Dixon, S., Rowan, A., Yan, Z., Campochiaro, P.A., and Semenza, G.L. (2003). Cell type-specific regulation of angiogenic growth factor gene expression and induction of angiogenesis in nonischemic tissue by a constitutively active form of hypoxia-inducible factor 1. Circ. Res. *93*, 1074–1081.

Kirsch, M., Schackert, G., and Black, P.M. (2000). Angiogenesis, metastasis, and endogenous inhibition. J. Neurooncol. *50*, 173–180.

Kurz, H., Fehr, J., Nitschke, R., and Burkhardt, H. (2008). Pericytes in the mature chorioallantoic membrane capillary plexus contain desmin and alpha-smooth muscle actin: relevance for non-sprouting angiogenesis. Histochem. Cell Biol. *130*, 1027–1040.

Lee, B.C., Lee, T.H., Avraham, S., and Avraham, H.K. (2004). Involvement of the chemokine receptor CXCR4 and its ligand stromal cell-derived factor 1alpha in breast cancer cell migration through human brain microvascular endothelial cells. Mol. Cancer Res. *2*, 327–338.

Li, J.L., Sainson, R.C., Shi, W., Leek, R., Harrington, L.S., Preusser, M., Biswas, S., Turley, H., Heikamp, E., Hainfellner, J.A., and Harris, A.L. (2007). Delta-like 4 Notch ligand regulates tumor angiogenesis, improves tumor vascular function, and promotes tumor growth in vivo. Cancer Res. *67*, 11244–11253.

Lobov, I.B., Brooks, P.C., and Lang, R.A. (2002). Angiopoietin-2 displays VEGF-dependent modulation of capillary structure and endothelial cell survival in vivo. Proc. Natl. Acad. Sci. USA *99*, 11205–11210.

Lu, C., Kamat, A.A., Lin, Y.G., Merritt, W.M., Landen, C.N., Kim, T.J., Spannuth, W., Arumugam, T., Han, L.Y., Jennings, N.B., et al. (2007). Dual targeting of endothelial cells and pericytes in antivascular therapy for ovarian carcinoma. Clin. Cancer Res. *13*, 4209–4217.

Mazzieri, R., Pucci, F., Moi, D., Zonari, E., Ranghetti, A., Berti, A., Politi, L.S., Gentner, B., Brown, J.L., Naldini, L., and De Palma, M. (2011). Targeting the ANG2/TIE2 axis inhibits tumor growth and metastasis by impairing angiogenesis and disabling rebounds of proangiogenic myeloid cells. Cancer Cell *19*, 512–526.

Mukherjee, D., and Zhao, J. (2013). The Role of chemokine receptor CXCR4 in breast cancer metastasis. American journal of cancer research *3*, 46–57.

Müller, A., Homey, B., Soto, H., Ge, N., Catron, D., Buchanan, M.E., McClanahan, T., Murphy, E., Yuan, W., Wagner, S.N., et al. (2001). Involvement of chemokine receptors in breast cancer metastasis. Nature *410*, 50–56.

Nasarre, P., Thomas, M., Kruse, K., Helfrich, I., Wolter, V., Deppermann, C., Schadendorf, D., Thurston, G., Fiedler, U., and Augustin, H.G. (2009). Host-derived angiopoietin-2 affects early stages of tumor development and vessel maturation but is dispensable for later stages of tumor growth. Cancer Res. *69*, 1324–1333.

O'Reilly, M.S., Holmgren, L., Shing, Y., Chen, C., Rosenthal, R.A., Moses, M., Lane, W.S., Cao, Y., Sage, E.H., and Folkman, J. (1994). Angiostatin: a novel angiogenesis inhibitor that mediates the suppression of metastases by a Lewis lung carcinoma. Cell *79*, 315–328.

O'Reilly, M.S., Boehm, T., Shing, Y., Fukai, N., Vasios, G., Lane, W.S., Flynn, E., Birkhead, J.R., Olsen, B.R., and Folkman, J. (1997). Endostatin: an endogenous inhibitor of angiogenesis and tumor growth. Cell *88*, 277–285.

Oh, H., Takagi, H., Suzuma, K., Otani, A., Matsumura, M., and Honda, Y. (1999). Hypoxia and vascular endothelial growth factor selectively up-regulate angiopoietin-2 in bovine microvascular endothelial cells. J. Biol. Chem. *274*, 15732–15739.

Orlidge, A., and D'Amore, P.A. (1987). Inhibition of capillary endothelial cell growth by pericytes and smooth muscle cells. J. Cell Biol. *105*, 1455–1462.

Pàez-Ribes, M., Allen, E., Hudock, J., Takeda, T., Okuyama, H., Viñals, F., Inoue, M., Bergers, G., Hanahan, D., and Casanovas, O. (2009). Antiangiogenic therapy elicits malignant progression of tumors to increased local invasion and distant metastasis. Cancer Cell *15*, 220–231.

Rigamonti, N., Kadioglu, E., Keklikoglou, I., Wyser Rmili, C., Leow, C.C., and De Palma, M. (2014). Role of angiopoietin-2 in adaptive tumor resistance to VEGF signaling blockade. Cell Rep. *8*, 696–706.

Saharinen, P., Eklund, L., Pulkki, K., Bono, P., and Alitalo, K. (2011). VEGF and angiopoietin signaling in tumor angiogenesis and metastasis. Trends Mol. Med. *17*, 347–362.

Scharpfenecker, M., Fiedler, U., Reiss, Y., and Augustin, H.G. (2005). The Tie-2 ligand angiopoietin-2 destabilizes quiescent endothelium through an internal autocrine loop mechanism. J. Cell Sci. *118*, 771–780.

Sennino, B., Falcón, B.L., McCauley, D., Le, T., McCauley, T., Kurz, J.C., Haskell, A., Epstein, D.M., and McDonald, D.M. (2007). Sequential loss of tumor vessel pericytes and endothelial cells after inhibition of platelet-derived growth factor B by selective aptamer AX102. Cancer Res. *67*, 7358–7367.

Skuli, N., Liu, L., Runge, A., Wang, T., Yuan, L., Patel, S., Iruela-Arispe, L., Simon, M.C., and Keith, B. (2009). Endothelial deletion of hypoxia-inducible factor-2alpha (HIF-2alpha) alters vascular function and tumor angiogenesis. Blood *114*, 469–477.

Skuli, N., Majmundar, A.J., Krock, B.L., Mesquita, R.C., Mathew, L.K., Quinn, Z.L., Runge, A., Liu, L., Kim, M.N., Liang, J., et al. (2012). Endothelial HIF-2α regulates murine pathological angiogenesis and revascularization processes. J. Clin. Invest. *122*, 1427–1443.

Song, S., Ewald, A.J., Stallcup, W., Werb, Z., and Bergers, G. (2005). PDGFRbeta+ perivascular progenitor cells in tumours regulate pericyte differentiation and vascular survival. Nat. Cell Biol. *7*, 870–879.

Srivastava, K., Hu, J., Korn, C., Savant, S., Teichert, M., Kapel, S.S., Jugold, M., Besemfelder, E., Thomas, M., Pasparakis, M., and Augustin, H.G. (2014). Postsurgical adjuvant tumor therapy by combining anti-angiopoietin-2 and metronomic chemotherapy limits metastatic growth. Cancer Cell *26*, 880–895.

Stahl, A., Connor, K.M., Sapieha, P., Chen, J., Dennison, R.J., Krah, N.M., Seaward, M.R., Willett, K.L., Aderman, C.M., Guerin, K.I., et al. (2010). The mouse retina as an angiogenesis model. Invest. Ophthalmol. Vis. Sci. *51*, 2813–2826.

Strasser, G.A., Kaminker, J.S., and Tessier-Lavigne, M. (2010). Microarray analysis of retinal endothelial tip cells identifies CXCR4 as a mediator of tip cell morphology and branching. Blood *115*, 5102–5110.

Suri, C., McClain, J., Thurston, G., McDonald, D.M., Zhou, H., Oldmixon, E.H., Sato, T.N., and Yancopoulos, G.D. (1998). Increased vascularization in mice overexpressing angiopoietin-1. Science *282*, 468–471.

Szarvas, T., Jäger, T., Tötsch, M., vom Dorp, F., Kempkensteffen, C., Kovalszky, I., Romics, I., Ergün, S., and Rübben, H. (2008). Angiogenic switch of angiopietins-Tie2 system and its prognostic value in bladder cancer. Clin. Cancer Res. *14*, 8253–8262.

Thomas, M., and Augustin, H.G. (2009). The role of the Angiopoietins in vascular morphogenesis. Angiogenesis *12*, 125–137.

Please cite this article in press as: Keskin et al., Targeting Vascular Pericytes in Hypoxic Tumors Increases Lung Metastasis via Angiopoietin-2, Cell Reports (2015), http://dx.doi.org/10.1016/j.celrep.2015.01.035

Thomas, M., Kienast, Y., Scheuer, W., Bähner, M., Kaluza, K., Gassner, C., Herting, F., Brinkmann, U., Seeber, S., Kavlie, A., et al. (2013). A novel angiopoietin-2 selective fully human antibody with potent anti-tumoral and anti-angiogenic efficacy and superior side effect profile compared to Pan-Angiopoietin-1/-2 inhibitors. PLoS ONE *8*, e54923.

Thurston, G., Suri, C., Smith, K., McClain, J., Sato, T.N., Yancopoulos, G.D., and McDonald, D.M. (1999). Leakage-resistant blood vessels in mice transgenically overexpressing angiopoietin-1. Science *286*, 2511–2514.

Thurston, G., Rudge, J.S., Ioffe, E., Zhou, H., Ross, L., Croll, S.D., Glazer, N., Holash, J., McDonald, D.M., and Yancopoulos, G.D. (2000). Angiopoietin-1 protects the adult vasculature against plasma leakage. Nat. Med. *6*, 460–463.

Vasudev, N.S., and Reynolds, A.R. (2014). Anti-angiogenic therapy for cancer: current progress, unresolved questions and future directions. Angiogenesis *17*, 471–494. http://dx.doi.org/10.1007/s10456-014-9420-y.

von Tell, D., Armulik, A., and Betsholtz, C. (2006). Pericytes and vascular stability. Exp. Cell Res. *312*, 623–629.

Weidner, N., Semple, J.P., Welch, W.R., and Folkman, J. (1991). Tumor angiogenesis and metastasis—correlation in invasive breast carcinoma. N. Engl. J. Med. *324*, 1–8.

Zetter, B.R. (1998). Angiogenesis and tumor metastasis. Annu. Rev. Med. *49*, 407–424.

Cell Reports

Supplemental Information

Targeting Vascular Pericytes in Hypoxic Tumors Increases Lung Metastasis via Angiopoietin-2

Doruk Keskin, Jiha Kim, Vesselina G. Cooke, Chia-Chin Wu, Hikaru Sugimoto, Chenghua Gu, Michele De Palma, Raghu Kalluri, and Valerie S. LeBleu

Supplemental Information

Supplemental Figures and Figure Legends

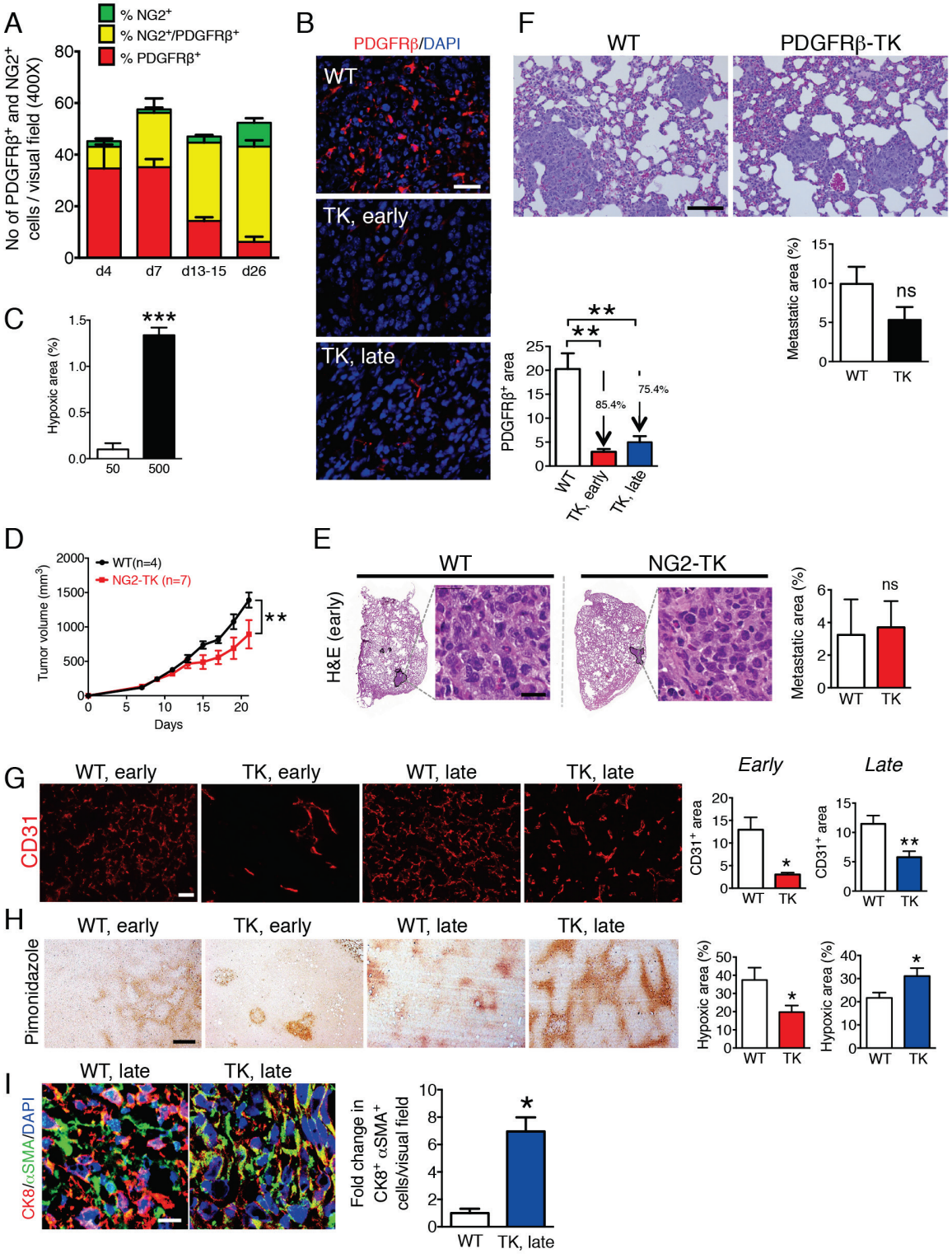

Figure S1. PDGFRβ$^+$ and NG2$^+$ pericyte recruitment in 4T1 tumor progression, related to Figure 1.

A Number of NG2$^+$, PDGFRβ$^+$, and NG2$^+$/PDGFRβ$^+$ double positive cells per field of view. d4, n=3; d7, n=3; d13-15, n=3; d26, n=5. **B** Representative images of tumors immunolabeled for PDGFRβ and quantification of the relative PDGFRβ$^+$ area in tumors with late (blue) and early (red) PDGFRβ$^+$ pericyte depletion. WT, n=8; PDGFRβ-TK early, n=5; PDGFRβ-TK late, n=4. Scale bar: 50 μm. Percentage differences in PDGFRβ$^+$ areas are listed relative to the WT group. **C** Percent hypoxic area in 50 and 500mm^3 4T1 orthotopic tumors. 50mm^3, n=3; 500mm^3, n=3. **D** Tumor volume measurements over time in mice with NG2$^+$ pericytes depletion beginning at an early stage of tumor progression. GCV treatment started before total tumor burden reached 100 mm^3. Two-way ANNOVA with Bonferroni's multiple comparison test was used. **E** H&E staining of lungs from the indicated experimental groups and quantification of the percent lung metastatic area. WT, n=4; NG2-TK, n=5. The metastatic nodules are encircled. High-magnification images of metastatic nodules are shown, scale bar: 25 μm. **F** H&E staining of lungs from wild-type (WT) and PDGFRβ-TK mice following 4T1 intravenous injection and respective quantification of the percent lung metastatic area. WT, n=8; PDGFRβ-TK, n=8. Scale bar: 100 μm. **G** Representative image of tumors immunolabeled for CD31 and quantification of the percent CD31$^+$ area per field of view. WT early, n=4; PDGFRβ-TK early, n=4; WT late, n=6; PDGFRβ-TK late, n=6. Scale bar: 50 μm. **H** Representative images of tumors immunolabeled for pimonidazole adduct formation (hypoxic area) in the indicated experimental groups and quantitation of the percent hypoxic area. WT early, n=7; PDGFRβ-TK early, n=8; WT late, n=10; PDGFRβ-TK late, n=14. Scale bar: 250 μm. **I** Representative images of tumors immunolabeled for CK8 and αSMA in the indicated experimental groups and quantification of

the relative $CK8^{+}\alpha SMA^{+}$ cells per visual field. WT, n=3; PDGFRβ-TK, n=3. Scale bar: 10 μm. Different images for this experiment are also shown in Figure 4G. Data are represented as the mean +/- SEM. Unless otherwise noted, unpaired two-tailed t-test was used to determine statistical significance. * $p<0.05$, ** $p<0.01$. ns: not significant.

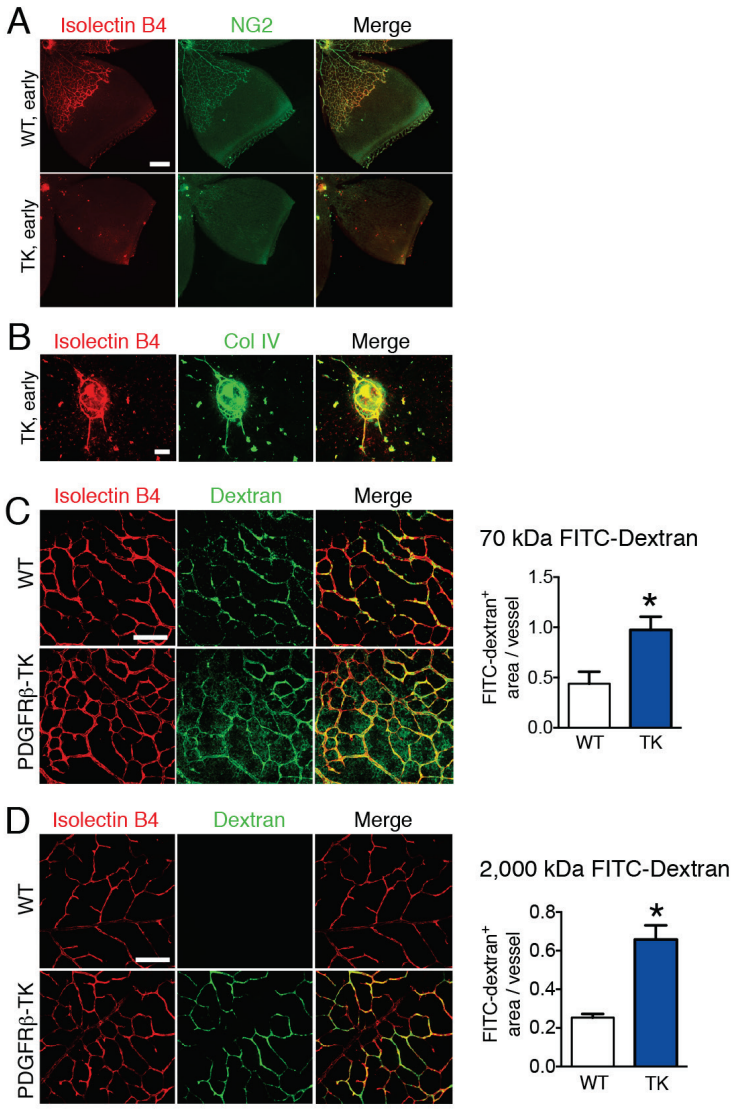

Figure S2. Vascular phenotype in retina angiogenesis with PDGFRβ$^+$ pericyte depletion, related to Figure 2.

A Immunolabeling for NG2 (pericytes marker) and Isolectin B4 staining in retina of WT and PDGFRβ-TK mice treated with GCV from P0 to P5 (early depletion) or from P4 to P9 (late depletion). Scale bar: 500 μm. **B** Immunolabeling for Collagen IV followed by Isolectin B4 staining of retinas from PDGFRβ-TK mice treated with GCV from P0 to P5. Scale bar: 100 μm. **C** Isolectin B4 staining and visualization of 70 kDa FITC-dextran in retina of WT and PDGFRβ-TK mice treated with GCV from P4 to P9 and quantitation of FITC-dextran$^+$ area per vessel. Scale bar: 100 μm. WT, n=3; PDGFRβ-TK, n=5. These data are also shown in Figure 2G. **D** Isolectin B4 staining and visualization of 2,000 kDa FITC-dextran in retina of WT and PDGFRβ-TK mice treated with GCV from P4 to P9 and quantitation of FITC-dextran$^+$ vessel. Scale bar: 100 μm. WT, n=3; PDGFRβ-TK, n=3. Data are represented as the mean +/- SEM. Unpaired two-tailed t-test was used to determine statistical significance. * $p<0.05$.

A

Rank	TK vs. WT, early ablation	TK vs. WT, late ablation
1	Relaxin signaling	IGF-1 signaling
2	Angiopoietin signaling	VEGF signaling
3	Growth hormone signaling	Growth hormone signaling
4	VEGF signaling	GM-CSF signaling
5	PDGF signaling	EGF signaling
6	HGF signaling	Angiopoietin signaling
7	GM-CSF signaling	PDGF signaling
8	IGF-1 signaling	VEGF family ligand-receptor interactions
9	VEGF family ligand-receptor interactions	Erythropoietin signaling
10	Erythropoietin signaling	HGF signaling

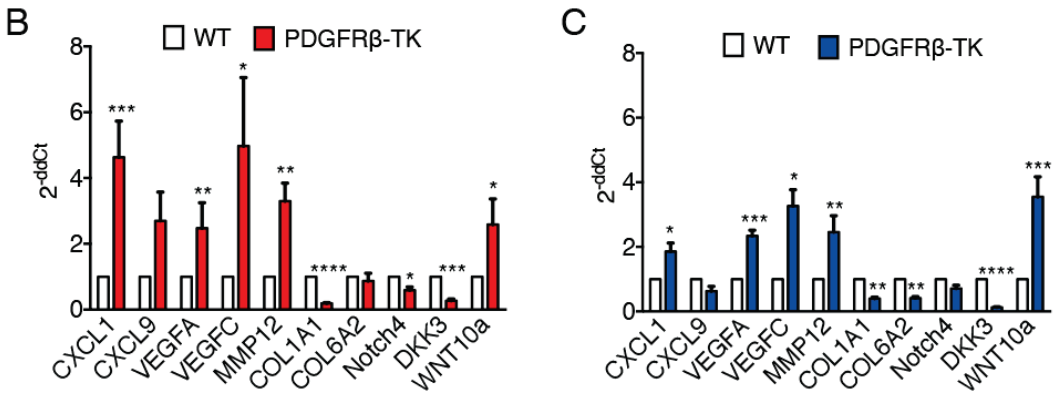

Figure S3. **Pathway analyses from global gene expression profiling and qRT-PCRs of differentially expressed genes in 4T1 tumors with early *vs.* late pericyte depletion, related to Figure 3.**

A Ranked list of top 10 growth factor signaling pathways based on the differentially expressed genes in 4T1 tumors from WT vs. PDGFRβ-TK mice with pericyte depletion in the early and late setting. **B-C** Transcript levels for the indicated genes assayed by quantitative RT-PCR in 4T1 tumors from WT and PDGFRβ-TK with early pericyte depletion (B) and late pericyte depletion (C). Data are represented as the mean +/- SEM. n > 3 in all groups was used. The control group (WT) was arbitrarily set to 1, unpaired one-tailed t-test. * $p<0.05$, ** $p<0.01$, *** $p< 0.001$, ****$p < 0.0001$.

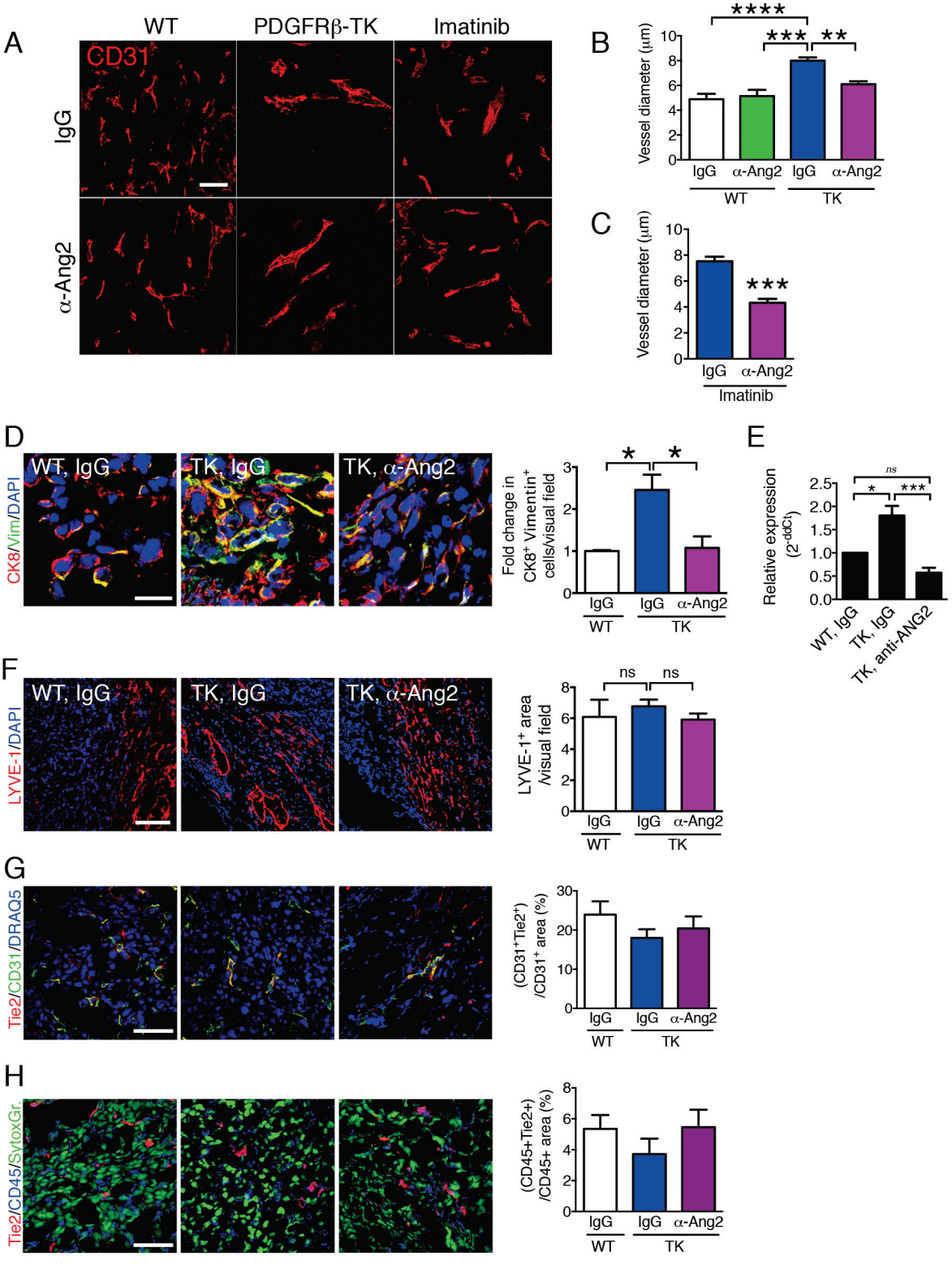
A
WT
PDGFRβ-TK
Imatinib
CD31
IgG
α-Ang2
B
Vessel diameter (μm)
IgG
α-Ang2
WT
TK
C
Imatinib
D
WT, IgG
TK, IgG
TK, α-Ang2
CK8/Vim/DAPI
Fold change in CK8+ Vimentin+ cells/visual field
E
Relative expression (2-ddCt)
WT, IgG
TK, IgG
TK, anti-ANG2
F
LYVE-1/DAPI
LYVE-1+ area /visual field
ns
G
Tie2/CD31/DRAQ5
(CD31+Tie2+) /CD31+ area (%)
H
Tie2/CD45/SytoxGr.
(CD45+Tie2+) /CD45+ area (%)

Figure S4. Anti-Ang2 antibody treatment restores vessel diameter in pericyte depleted tumors and suppresses EMT, related to Figure 4.

A Immunolabeling for CD31 in the tumors of the indicated experimental groups. Scale bar: 50 μm. **B-C** Quantification of the mean vessel diameter. B: IgG + WT, n=4; anti-ANG2 + WT, n=3; IgG + PDGFRβ-TK, n=5; anti-ANG2 + PDGFRβ-TK, n=5. One-way ANOVA with Tukey post-hoc analysis. C: IgG + Imatinib, n=4; anti-ANG2 + Imatinib, n=4. Unpaired two-tailed t-test. **D** Representative images of tumors immunolabeled for CK8 and Vimentin (Vim) in the indicated experimental groups and quantification of the relative $CK8^{+}Vim^{+}$ cells per visual field. WT, n=3; PDGFRβ-TK, n=4; anti-ANG2 + PDGFRβ-TK, n=3. Scale bar: 10 μm. **E** *Twist* transcript levels in 4T1 tumors from WT, PDGFRβ-TK and anti-ANG2 + PDGFRβ-TK mice (n=4 in each group). The control group (WT) was arbitrarily set to 1, unpaired one-tailed t-test. **F** Representative images of tumors immunolabeled for LYVE-1 in the indicated experimental groups and quantification of the percent $LYVE\text{-}1^{+}$ area per field of view. WT, n=3; PDGFRβ-TK, n=3; anti-ANG2 + PDGFRβ-TK, n=3. Scale bar: 100 μm. **G** Representative images of tumors immunolabeled for TIE2 and CD31 in the indicated experimental groups and quantification of the relative percentage of $TIE2^{+}CD31^{+}$ vessels per visual field. WT, n=3; PDGFRβ-TK, n=3; anti-ANG2 + PDGFRβ-TK, n=3. Scale bar: 50 μm. **H** Representative images of tumors immunolabeled for TIE2 and CD45 in the indicated experimental groups and quantification of the relative percentage of $TIE2^{+}CD45^{+}$ macrophages per visual field. WT, n=3; PDGFRβ-TK, n=3; anti-ANG2 + PDGFRβ-TK, n=3. Scale bar: 50 μm. Data are represented as the mean +/- SEM. Unless otherwise noted, one-way ANOVA with Tukey post-hoc analysis was used to determine statistical significance. * $p<0.05$, ** $p<0.01$, *** $p< 0.001$, **** $p < 0.0001$. ns: not significant.

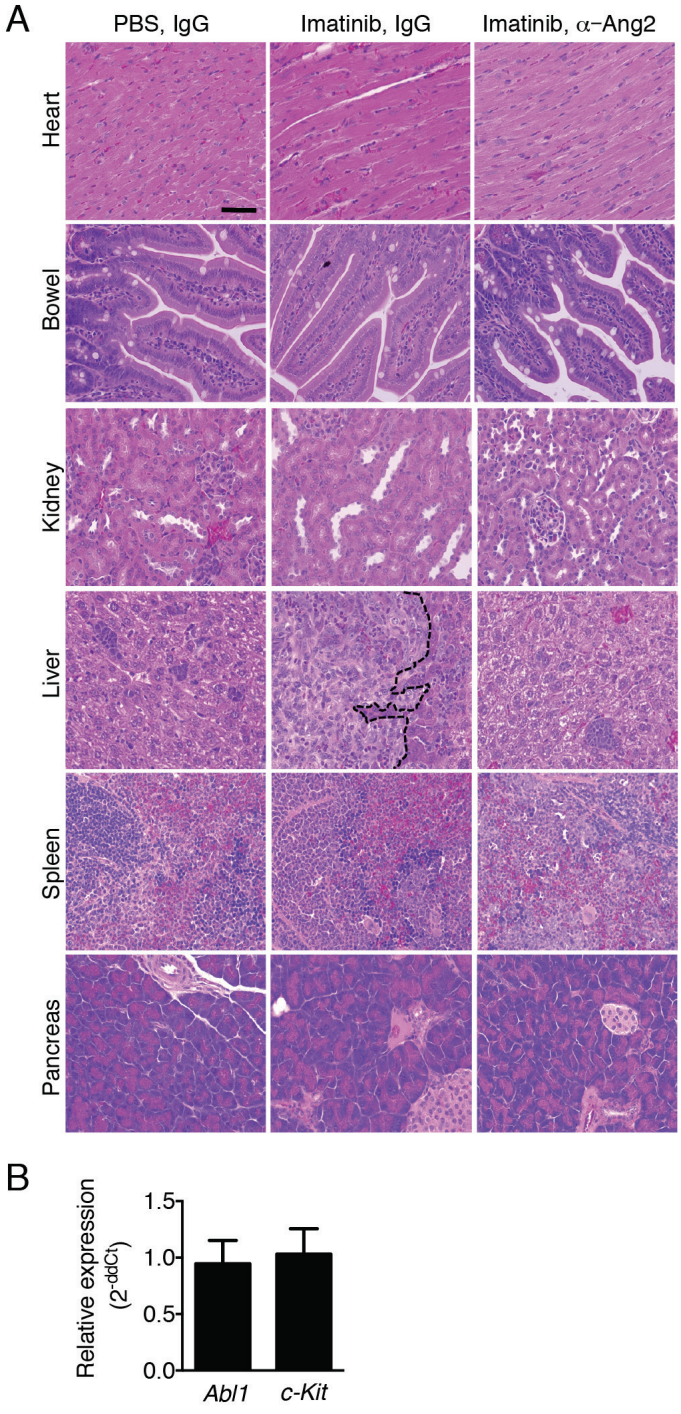

Figure S5. Imatinib and Anti-Ang2 antibody treatments present limited off target side effects, related to Figure 6.

A Representative H&E stained organs in the indicated experimental groups. A liver metastasis is delineated with a black dotted line. Scale bar: 50 μm. **B** Transcript levels of the indicated genes in 4T1 tumors from mice treated with Imatinib relative to control (PBS treated) mice. n=5 for each group, the control group (WT) was arbitrarily set to 1, and unpaired one-tailed t-test was used. Data are represented as the mean +/- SEM.

Supplementary Table

Table S1. Primer sequences used in this study, related to Figure 3.

Vegfa-qrtF	GCACATAGAGAGAATGAGCTTCC
Vegfa-qrtR	CTCCGCTCTGAACAAGGCT
Vegfc-qrtF	GAGGTCAAGGCTTTTGAAGGC
Vegfc-qrtR	CTGTCCTGGTATTGAGGGTGG
COL1A1-qrtF	GCTCCTCTTAGGGGCCACT
COL1A1-qrtR	CCACGTCTCACCATTGGGGG
COL6A2-qrtF	AAGGCCCCATTGGATTCCC
COL6A2-qrtR	CTCCCTTCCGACCATCCGAT
MMP12-qrtF	GAGTCCAGCCACCAACATTAC
MMP12-qrtR	GCGAAGTGGGTCAAAGACAG
Dkk3-qrtF	TCAGGAGGAAGCTACGCTCAA
Dkk3-qrtR	GTTCACCTCAGAGGACGTTTTAG
CXCL1-qrtF	CAGGGTCAAGGCAAGCCTC
CXCL1-qrtR	CTGGGATTCACCTCAAGAACATC
CXCL9-qrtF	TCCTTTTGGGCATCATCTTCC
CXCL9-qrtR	TTTGTAGTGGATCGTGCCTCG
Ang1-qrtF	CACATAGGGTGCAGCAACCA
Ang1-qrtR	CGTCGTGTTCTGGAAGAATGA
Ang2-qrtF	AGCAGATTTTGGATCAGACCAG
Ang2-qrtR	GCTCCTTCATGGACTGTAGCTG
Wnt10a-qrtF	CCTGTTCTTCCTACTGCTGCTGG
Wnt10a-qrtR	CGATCTGGATGCCCTGGATAGC
Notch4-qrtF	CTCTTGCCACTCAATTTCCCT
Notch4-qrtR	TTGCAGAGTTGGGTATCCCTG
CXCR4-qrtF	GACTGGCATAGTCGGCAATG
CXCR4-qrtR	AGAAGGGGAGTGTGATGACAAA
c-Kit-qrtF	GCCACGTCTCAGCCATCTG
c-Kit-qrtR	GTCGGGATCAATGCACGTCA
Abl1-qrtF	AAGGGGCTCTCTTCGTCCTC
Abl1-qrtR	AGAGTGCCACAAAAAGGTTGG
Twist-qrtF	CTGCCCTCGGACAAGCTG
Twist-qrtR	CTAGTGGGACGCGGACAT
ARP/36B4-qrtF	GGAGCCAGCGAGGCCACACTGCTG
ARP/36B4-qrtR	CTGGCCACGTTGCGGACACCCTCC
GAPDH-qrtF	AGGTCGGTGTGAACGGATTTG
GAPDH-qrtR	TGTAGACCATGTAGTTGAGGTCA

Supplemental Experimental Procedures

4T1 orthotopic and intravenous mammary cancer model and agent administration

PDGFRβ-TK or littermate control female mice, between the ages of 6 and 12 weeks, were used for orthotopic implantation of 4T1 mammary epithelial cancer cells (0.5 x 10^6 in each breast pad). Data from a subset of the PDGFRβ-TK mice in the late pericyte depletion experiments shown in Figure 1 was reported in our previous studies (Cooke et al., 2012). Ganciclovir (GCV, Invivogen) treatments were initiated once the average tumor burden reached 500 mm^3 for the late depletion group and before the average total tumor burden reached 100 mm^3 for the early depletion group. Mice received daily intraperitoneal (i.p.) GCV injections at a 50 mg/kg body weight (BW) dose. Tumor volumes were measured every 2-3 days using Vernier calipers and volumes were calculated using the formula (length x $width^2$ x $\pi/6$). Mice were euthanized when the tumor size of control mice reached approximately 2,500 mm^3. Mice also received i.p. injections of the neutralizing anti-ANG2 antibody (LC06, Roche Diagnostics) or control isotype matched IgG antibody once a week (10 mg/kg BW in 0.2 ml PBS) (Thomas et al., 2013), or imatinib or PBS by oral gavage daily (50 mg/kg BW in 0.1 ml). For intravenous injection, 0.5 x 10^6 4T1 cells were injected in the retro-orbital venous plexus and mice euthanized 7 days post cancer cell injection. In this setting, GCV injections were initiated 3 days before cancer cell injection. Mice were also injected i.p. with a single dose of hypoxyprobe (60 mg/kg BW in 0.5 ml of pimonidazole, HPI Inc.) 30 minutes before euthanasia.

Newborn mice treatment for retina experiments

PDGFRβ-TK or littermate control newborn mice were treated with GCV dissolved in PBS from P0 to P5 (early treatment) or P4 to P9 (late treatment). Ganciclovir (50 mg/kg BW in 10 μl) was

administered by i.p. injection daily for 5 consecutive days. Under anesthesia, 100 μl of 10mg/ml FITC-dextran (2,000 kDa or 70 kDa, Sigma) was injected intracardially and allowed to circulate for 5 minutes. The pups were euthanized by decapitation and the retinas as well as other organs were collected for further analysis. PDGFRβ-TK pups were also treated with anti-ANG2 or control anti-IgG antibodies in combination with GCV. Anti-ANG2 or anti-IgG was administered intraperitoneally once at P4 (10 mg/kg BW, at a volume of 10 μl) and GCV (50 mg/kg, at a volume of 10 μl) was administered daily by intraperitoneal injection until sacrifice (P9).

Quantification of metastatic burden and tumor necrosis

Hematoxylin and eosin staining of lung sections from paraffin-embedded tissue was generated by the BIDMC and MDACC histology core facilities. Image of an entire lobe of the lung was obtained using the Aperio Slide Scanner. Metastases were identified via histopathological analysis based on H&E staining and metastatic area was quantified by NIH ImageJ software as a percentage of total lung area. High magnification images (original magnification x100 or x90) of the metastatic area are provided for each lung photomicrographs. Tumor necrosis was assayed on Hematoxylin counter stained whole tumor cross-section and quantified by NIH ImageJ software as a percentage of total tumor area.

Immunostaining

Harvested tumors and lungs were fixed in 10% neutral buffered formalin, dehydrated, and embedded in paraffin. For hypoxyprobe immunohistochemistry, the deparaffinized tumor sections were incubated in 10 mM citrate buffer (pH 6.0) for 1 hour at boiling temperature prior to blocking with M.O.M. Mouse IgG Blocking Reagent (Vector Laboratories, West Grove, PA)

for 1 hour. Sections were incubated with Hypoxyprobe™ antibody (1:50, HPI Inc.) overnight at 4°C, followed by incubation with biotin-conjugated anti-rabbit/rat/mouse IgG and ABC reagent (Vector Laboratories, West Grove, PA) for 30 min each at room temperature. The sections were then developed by DAB staining according to the manufacturer's instructions. Images were obtained by either light microscopy at 4X magnification or the Aperio Slide Scanner. DAB (brown) positivity was analyzed in ≥3 fields/tumor by NIH ImageJ analysis software at an original magnification of X4 or on scanned tumor images. Control and treated mice within an experimental set (3 or more tumors/group) were analyzed and results reported as staining area per tumor section or percent staining per visual field (4X). Alternatively, harvested tumors and lungs were embedded in O.C.T. medium (TissueTek, Torrance, CA), and immunostainings were performed on frozen sections. Frozen sections were fixed in either 4% PFA for 5 minutes or acetone for 10 minutes at 4°C and blocked one hour with 5% donkey or goat serum in PBST at room temperature. Following blocking, sections were incubated in 1:50 rat anti-PDGFRβ (eBiosciences), 1:200 rabbit anti-NG2 (Millipore), 1:300 desmin, 1:100 CD31 (DSHB), 1:100 CD31 (BD Pharmingen), 1:200 Collagen IV (MP Biomedicals), 1:50 CK8 (DSHB), 1:200 αSMA (Sigma), 1:100 ZO-1 (Invitrogen), 1:100 FITC (AbD Serotec), 1:200 LYVE-1 (AngioBio), 1:100 Vimentin (Cell Signaling), at 4°C overnight, followed by fluorescent secondary antibodies. Slides were mounted with either DAPI, DRAQ5 (Molecular Probe), or Sytox Green staining, to label the nuclei. For Figure S4G-H, 1:50 PE-conjugated anti-TIE2 (eBiosciences) was used with Tyramide Signal Amplification (TSA) Systems (PerkinElmer), followed by immunoableing with 1:50 FITC-conjugated anti-CD31 (BD Pharmingen) or 1:100 APC-conjugated anti-CD45 (BD Pharmingen). Positive staining was quantified in ≥3 visual fields/tumor at original magnification x20, x40 or x63 using NIH ImageJ software, where the

same threshold was used for all compared conditions to determine the positive staining area fractions per field. Three to eight tumors/group were used in the assessments. For data presented in Figure 1C & H-I, the WT group contained WT mice treated with GCV early and late. Statistical analysis was done using the average staining area fraction per tumor. Stainings were visualized on either the Zeiss Axioskop 2 microscope or the Zeiss LSM 510 Meta Confocal microscope. Quantification of the number of $PDGFR\beta^+/NG2^+$ double-positive cells (4 fields/tumor and 4 mice/group) was performed by NIH-ImageJ cell counter application and reported as percent co-localization per visual field. The number of pericytes that are associated with vessels were determined by ImageJ cell counter application under original magnification x40 and reported as percentage of vessels that have associated pericytes out of the total number of vessels, per visual field. Percent pericyte coverage was determined by the following formula: Number of pericyte-associated $CD31^+$ vessels/field divided by the total number of $CD31^+$ vessels/field multiplied by 100. Quantification of the relative percentage of $TIE2^+CD31^+$ vessels and $TIE2^+/CD45^+$ macrophages (6 fields/tumor and 3 mice/group) was performed by NIH-ImageJ and reported as relative percent co-localization over total CD31 or CD45 positive area per visual field.

In situ hybridization

In situ hybridization (ISH) was performed on frozen 4T1 tumor sections using standard methods. Briefly, frozen tumor sections (4-6 tumors/group) were cut into 10 μm-thick sections using a cryostat (Leica), post-fixed in 4% PFA, acetylated in 1% triethanolamine and 0.25% acetic anhydride, pre-hybridized, then hybridized with *ANG2* probe overnight at 65°C. After hybridization, sections were washed and incubated with AP-conjugated sheep anti-DIG antibody

(1:1000; Roche) for 90 min at room temperature. After three washes, sections were incubated in BM Purple (Roche) until positive staining was seen. Digoxigenin labeled *ANG2 in situ* riboprobes were generated by *in vitro* transcription method (Promega and Roche). ANG2 plasmid construct for generating the probes was provided by Anne Eichmann (Yale University School of Medicine). Immunostaining for Collagen IV and CD31 was performed after this step, as previously described. Images were obtained at x20 magnification. Quantification for *ANG2* signal was performed by NIH ImageJ software, where the same threshold was used for all compared conditions to determine the positive staining area fractions per field. The results reported as positive staining area fraction per field.

Immunohistochemistry of whole-mount retinas

Eyes harvested from the pups were prefixed in 4% paraformaldehyde (PFA) for 10 min at room temperature. Retinas dissected in PBS were post-fixed in 4% PFA overnight at 4°C. Permeabilization of retinas were done in PBS, 0.5% Triton X-100, and 1% normal goat serum overnight at 4°C. After blocking in blocking buffer (PBS, 0.5% Triton X-100, 10% normal goat serum) for 1 hr at room temperature, retinas were incubated with primary antibody (NG2, PDGFRβ, Collagen IV and CD31, as described above) in blocking buffer overnight at 4°C. After washing in PBS/0.5% Triton X-100 for 2–3 hrs, retinas were incubated in Alexa Fluor-conjugated secondary antibody then washed several times. Retinas were then washed twice in PBlec (PBS at pH 6.8, 1% Triton X-100, 0.1 mM $CaCl_2$, 0.1 mM $MgCl_2$, 0.1 mM $MnCl_2$) and incubated in Isolectin B4 (1:500; I21411, Molecular Probes) in PBlec overnight at 4°C. The retinas were flat-mounted using ProLong Gold/DAPI anti-fade reagent (P36935, Molecular Probes), following a wash in PBS and a brief post-fixation in PFA. Flat-mounted retinas were

analyzed by fluorescence microscopy using a Nikon Eclipse 80i or Zeiss Axioskop 2 microscope equipped with a Nikon DS-2 digital camera or by confocal laser-scanning microscopy using a Zeiss LSM 510 META. Images were processed using Adobe Photoshop and ImageJ software.

Analysis of postnatal retinal angiogenesis

Images of whole mount retinas were taken at 10x magnification to measure vessel density. The number of branch points per field (100 X 100 μm fields, images taken with 10X magnification, 3 fields/retina and 3-4 retinas/group) at the periphery of vasculature was quantified using Image J. FITC-dextran was visualized directly by fluorescent microscopy under the green fluorescent filter and quantified by ImageJ area fraction analysis. 3-8 fields/retina and 3-4 retinas / group were analyzed at original magnification x10. Vessel diameter was measured at original magnification x63 and 8-10 fields/ retina and 3-4 retinas / group was analyzed.

ELISA

Tumors were lysed in 300-600 μl of PBS supplemented with proteinase inhibitors (Roche) on ice. The lysate was then subjected to 2 freeze-thaw cycles then spun for 15 min at 5000 rpm at 4°C. The lysate was cleared with a second centrifugation for 15 min at 10,000 rpm at 4°C. The protein lysate was quantified using the BCA protein assay reagents (Pierce), accordingly to manufacturer's directions. 50 μg of lysates was diluted in the sample diluent buffer provided in the Angiopoietin-2 Mouse ELISA Kit (Abcam) and the ELISA was then carried out following the manufacturer's directions.

Microarray analysis and quantitative PCR analyses

Total RNA was isolated from 4T1 tumors implanted in WT+GCV late (n=4) and PDGFRβ-TK+GCV late mice (n=4) or WT+GCV early (n=8) and PDGFRβ-TK+GCV early mice (n=8) using RNeasy Plus Mini Kit (Qiagen), and equal amount of RNA from each tumors in each group was pooled together, and submitted to the Molecular Genetics Core Facility at Children's Hospital (Boston, MA). Microarray analysis was performed using Mouse Ref8 Gene Expression BeadChip (Illumina), and gene expression was determined by MetaCore (GeneGo) and Genome Studio (Illumina) software. Ingenuity Pathway Analysis (IPA) was performed on the microarray data set, with a threshold of 1.2 fold. Total RNA was also isolated from 4T1 tumors implanted in WT mice treated with GCV and anti-IgG (n=3), PDGFRβ-TK mice treated with GCV and anti-IgG mice (n=3), and PDGFRβ-TK mice treated with GCV and anti-ANG2 antibody (n=3) using RNeasy Plus Mini Kit (Qiagen) and submitted to the Molecular Genetics Core Facility at MDACC. Gene expression analysis was performed using Mouse Ref6 Gene Expression BeadChip (Illumina), and the Limma package from R Bioconductor (Gyorffy et al., 2012) was used to analyze differentially expressed genes. Pathway analysis was performed using Ingenuity Pathway Analysis (IPA). All microarray data were deposited in Gene Expression Omnibus under the accession number GSE55785. For RT PCR analyses, tumor or retina tissue samples were homogenized in Trizol® (Invitrogen) and RNA was extracted according to manufacturer's instructions. cDNA was generated using the High Capacity cDNA Reverse Transcriptase Kit (Applied Biosystems). Gene Expression was determined using the Applied Biosystems 7300 Sequence Detector System and SYBR green as the fluorescence reporter. Measurements were standardized to the housekeeping genes (ARP/36B4 or GAPDH). Primer sequence information is listed in Table S1.

Kaplan-Meier plotter analyses (Gyorffy et al., 2012)

The *Angpt1* Affymetrix ID 205608_s_at, *Angpt2* Affymetrix ID 211148_s_at, and Pdgfrb Affymetrix ID 202273_at were used as selected probe set for analysis of 3455 patient transcriptome with known recurrence free survival (the 2014 version of the database was used). Patients were split by median expression and selection criteria was not further restricted by subtypes or treatment. Both hazard ratio (HR) and Log-Rank test P value are listed.

Supplemental References

Cooke, V. G., LeBleu, V. S., Keskin, D., Khan, Z., O'Connell, J. T., Teng, Y., Duncan, M. B., Xie, L., Maeda, G., Vong, S*., et al.* (2012). Pericyte depletion results in hypoxia-associated epithelial-to-mesenchymal transition and metastasis mediated by met signaling pathway. Cancer cell *21*, 66-81.

Gyorffy, B., Lanczky, A., and Szallasi, Z. (2012). Implementing an online tool for genome-wide validation of survival-associated biomarkers in ovarian-cancer using microarray data from 1287 patients. Endocrine-related cancer *19*, 197-208.

Thomas, M., Kienast, Y., Scheuer, W., Bahner, M., Kaluza, K., Gassner, C., Herting, F., Brinkmann, U., Seeber, S., Kavlie, A*., et al.* (2013). A novel angiopoietin-2 selective fully human antibody with potent anti-tumoral and anti-angiogenic efficacy and superior side effect profile compared to Pan-Angiopoietin-1/-2 inhibitors. PloS one *8*, e54923.